



Contents lists available at ScienceDirect

Bioorganic & Medicinal Chemistry

journal homepage: www.elsevier.com/locate/bmc

BET bromodomain ligands: Probing the WPF shelf to improve BRD4 bromodomain affinity and metabolic stability

Laura E. Jennings^{a,1}, Matthias Schiedel^{a,1}, David S. Hewings^a, Sarah Picaud^b, Corentine M.C. Laurin^a, Paul A. Bruno^{c,d,e}, Joseph P. Bluck^{a,f}, Amy R. Scorch^a, Larissa See^a, Jessica K. Reynolds^a, Mustafa Moroglu^a, Ishna N. Mistry^g, Amy Hicks^a, Pavel Guzanov^a, James Clayton^a, Charles N.G. Evans^a, Giulia Stazi^h, Philip C. Biggin^f, Anna K. Mapp^{c,d,e}, Ester M. Hammond^g, Philip G. Humphreysⁱ, Panagis Filippakopoulos^b, Stuart J. Conway^{a,*}

^a Department of Chemistry, Chemistry Research Laboratory, University of Oxford, Mansfield Road, Oxford OX1 3TA, United Kingdom

^b Nuffield Department of Clinical Medicine, Structural Genomics Consortium, University of Oxford, Old Road Campus Research Building, Roosevelt Drive, Oxford OX3 3TA, United Kingdom

^c Department of Chemistry, University of Michigan, Ann Arbor, MI 48109-1055, United States

^d Life Sciences Institute, University of Michigan, Ann Arbor, MI 48109-2216, United States

^e Program in Chemical Biology, University of Michigan, Ann Arbor, MI 48109-2216, United States

^f Department of Biochemistry, University of Oxford, South Parks Road, Oxford OX1 3QU, United Kingdom

^g CRUK/MRC Oxford Institute for Radiation Oncology, Department of Oncology, University of Oxford, Old Road Campus Research Building, Oxford OX3 7DQ, United Kingdom

^h Department of Chemistry and Technologies of Drugs, Sapienza University of Rome, Piazzale Aldo Moro 5, 00185 Rome, Italy

ⁱ Epigenetics Discovery Performance Unit, GlaxoSmithKline R&D, Stevenage Hertfordshire SG1 2NY, United Kingdom

ARTICLE INFO

Article history:

Received 23 February 2018

Revised 30 April 2018

Accepted 2 May 2018

Available online xxx

ABSTRACT

Ligands for the bromodomain and extra-terminal domain (BET) family of bromodomains have shown promise as useful therapeutic agents for treating a range of cancers and inflammation. Here we report that our previously developed 3,5-dimethylisoxazole-based BET bromodomain ligand (OXFBD02) inhibits interactions of BRD4(1) with the RelA subunit of NF- κ B, in addition to histone H4. This ligand shows a promising profile in a screen of the NCI-60 panel but was rapidly metabolised ($t_{1/2}$ = 39.8 min). Structure-guided optimisation of compound properties led to the development of the 3-pyridyl-derived OXFBD04. Molecular dynamics simulations assisted our understanding of the role played by an internal hydrogen bond in altering the affinity of this series of molecules for BRD4(1). OXFBD04 shows improved BRD4(1) affinity (IC_{50} = 166 nM), optimised physicochemical properties (LE = 0.43; LLE = 5.74; SFI = 5.96), and greater metabolic stability ($t_{1/2}$ = 388 min).

© 2018 The Authors. Published by Elsevier Ltd. This is an open access article under the CC BY-NC-ND license (<http://creativecommons.org/licenses/by-nc-nd/4.0/>).

1. Introduction

Lysine acetylation is a prevalent protein post-translational modification (PTM) that occurs throughout the proteome¹ and is similar to phosphorylation in its ability to regulate protein function.² The role of acetyl-lysine (KAc) has been heavily studied in histone proteins, with KAc recognised as one of the key “marks” proposed to comprise the epigenetic code.^{3,4} Lysine acetylation state is regulated by lysine acetyl transferases (KATs) and lysine deacetylases (KDACs), while bromodomains are viewed as readers of KAc marks, and mediate chromatin-protein interactions that are frequently involved in transcriptional regulation.⁵ There are 61

bromodomains found within 46 bromodomain-containing proteins (BCPs) in the human proteome which, despite having diverse primary sequences, share a common protein fold and structure.⁶ The KAc residue binds in a well-defined pocket that, in some bromodomains, contains 5 structurally-conserved water molecules at its base, and possesses a key recognition residue that hydrogen bonds to the KAc; in canonical bromodomains this is an Asn residue. A sustained effort over recent years has resulted in small-molecule ligands being identified for an increasing number of these bromodomains.^{7–12} The majority of work has focused on the development of ligands for the bromodomain and extra terminal domain (BET) family of BCPs, comprising bromodomain-containing proteins 2–4 (BRD2–4) and the testis-specific BRDT; each of these proteins contains two adjacent canonical bromodomains. There is also increasing work on the development of ligands for the non-BET bromodomains.^{13–16} The BET bromodomains have emerged

* Corresponding author.

E-mail address: stuart.conway@chem.ox.ac.uk (S.J. Conway).

¹ These authors contributed equally to this work.

<https://doi.org/10.1016/j.bmc.2018.05.003>

0968-0896/© 2018 The Authors. Published by Elsevier Ltd.

This is an open access article under the CC BY-NC-ND license (<http://creativecommons.org/licenses/by-nc-nd/4.0/>).

as exciting therapeutic targets with over 20 clinical trials involving BET bromodomain ligands in progress, primarily focused on oncology indications.^{14,17–19} Here we report further cellular data for our previously reported BET bromodomain ligand OXFBD02 (**1**),^{20,21} and subsequent structure-activity relationship (SAR) studies aimed at optimising the solubility and metabolic stability of this series of compounds. This work resulted in the development of OXFBD04 (**9j**), which displays improved BRD4(1) affinity and substantially enhanced metabolic stability compared to OXFBD02.

2. Results and discussion

A common feature of almost all bromodomain ligands is a component that occupies the KAc-binding pocket and mimics the interactions formed by KAc with the bromodomain. Work by us^{20–25} and others^{26–35} has shown that the 3,5-dimethylisoxazole group is a particularly effective KAc mimic, which has been used as the basis of ligands for the CREBBP bromodomain and the BET family of BCPs (Fig. 1).

Using a fragment-based approach we previously developed OXFBD02 (**1a**) and OXFBD03 (**1b**) which have IC₅₀ values of 384 nM and 371 nM in an AlphaScreen assay for the first bromodomain of BRD4 [BRD4(1)], and IC₅₀ values for cytotoxicity of 794 nM and 616 nM in the MV4;11 acute myeloid leukaemia (AML) cell line, respectively.^{20,21}

2.1. Cellular evaluation of OXFBD02 (**1**)

To determine its activity against a wider panel of cancer cell lines, OXFBD02 (**1a**) was submitted for testing at a single dose against the NCI-60 human cancer cell line screen.³⁸ Growth inhibition (GI) was determined after 48 h treatment at 10 μM, using a

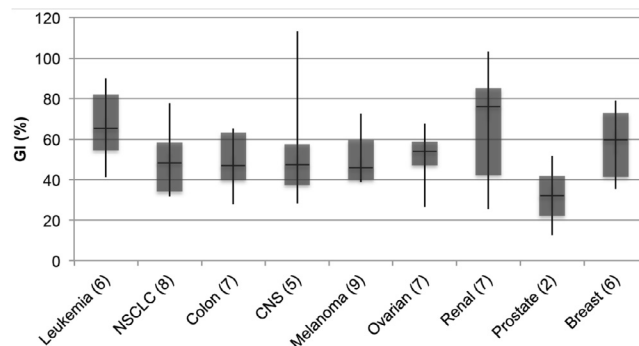


Fig. 2. Box plot of growth inhibition (GI) by OXFBD02 (**1a**) in NCI-60 panel. Plot indicates median, range and quartiles of GI by **1a** after 48 h treatment at 10 μM in the NCI-60 DTP Human Tumour Cell Screen, grouped by cancer type. The number in brackets is the number of cell lines of each type in the NCI-60 panel. (Graphical representation in analogy to Lucas et al.)³⁹.

sulforhodamine B assay (to indicate cellular protein content). The compound was subsequently evaluated at five concentrations between 10 nM and 100 μM to obtain GI₅₀ values, and to indicate the concentration required (if < 100 μM) for total growth inhibition (TGI) (Table S1). A box plot of the data grouped by cancer type is shown (Fig. 2).

Similar to other BET bromodomain ligands, OXFBD02 (**1a**) was particularly effective at inhibiting the growth of leukaemia-, breast-, and renal-cancer cell lines. Calculation of the GI₅₀ values (see Table S1) allow comparison of OXFBD02 (**1a**) with the NCI-60 data obtained for PFI-1 (**7**, see Fig. 1), which is a chemically-distinct well-characterised BET bromodomain ligand.³⁶ PFI-1 (**7**) and OXFBD02 (**1a**) display well correlated patterns of cancer cell

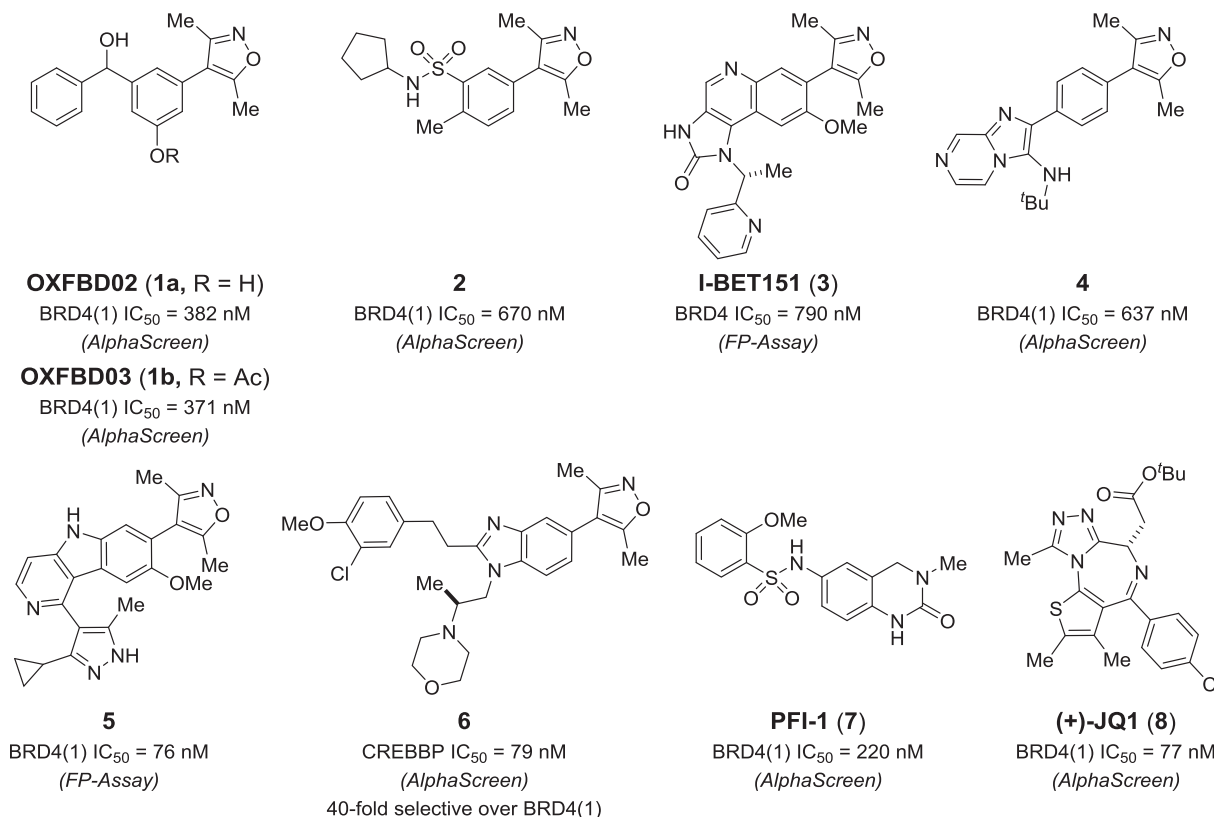


Fig. 1. Chemical structures and *in vitro* inhibition data of the 3,5-dimethylisoxazole-based BET bromodomain ligands **1–5**,^{21,26,27,31,33,34} the 3,5-dimethylisoxazole-based CREBBP bromodomain ligand **6**,²⁴ and the structurally unrelated BET bromodomain ligands PFI-1 (**7**)³⁶ and (+)-JQ1 (**8**)³⁷.

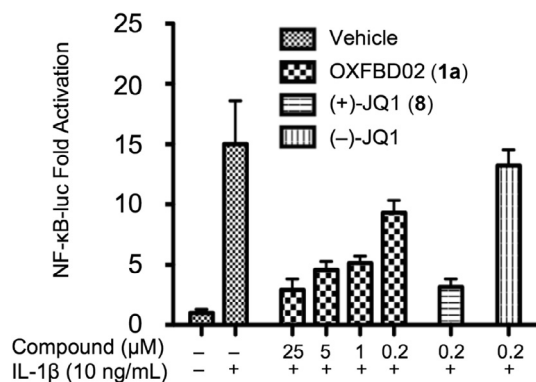


Fig. 3. Luciferase reporter gene assay allows assessment of the effect of compounds on NF-κB-dependent gene expression. HeLa cells were transiently transfected with a reporter plasmid containing luciferase and five κB binding sites. The cells were treated with DMSO as a control (–), or different concentrations (0.2, 1, 5 and 25 μM) of OXFBD02 (**1a**), (+)-JQ1 (**8**), or (–)-JQ1 for 12 h before stimulation with IL-1β (+). The gene expression without stimulation of IL-1β (–) was also measured for the DMSO-treated control. Results were obtained in quadruplicate and averaged, with error bars signifying standard deviation. OXFBD02 (**1a**) shows a concentration-dependent effect on transcription.

toxicity (Pearson's product-moment correlation coefficient, $r = 0.82$; Table S1, Fig. S1 and S2).³⁶ These data suggest that the activity displayed by both compounds results predominantly from interaction with the BET bromodomains, rather than other chemotype-specific off-target cellular interactions.

Beyond its interactions with KAc residues in histone proteins, BRD4 has been reported to bind KAc310 of the RelA subunit of NF-κB. The binding of BRD4 leads to recruitment of cyclin-dependent kinase 9 (CDK9), phosphorylation of RNA polymerase II, and consequent activation of NF-κB-dependent gene expression.^{40–43} Disruption of the RelA-BRD4 interaction with the BET ligand (+)-JQ1 (**8**) was previously shown to suppress NF-κB-dependent transcription.⁴¹ To investigate whether OXFBD02 (**1a**) also disrupts the interaction of BET bromodomains KAc310 of RelA, and to assess the cellular effects of OXFBD02 (**1a**) in a functional assay, we employed a luciferase reporter system based on a previously published procedure.⁴⁴ This allowed us to determine the effects of BRD4 bromodomain binding on NF-κB-dependent transcription. (+)-JQ1 (**8**, see Fig. 1) was employed as a positive control and exerted a potent suppression of NF-κB-dependent gene expression, whereas the inactive enantiomer (–)-JQ1 did not show significant effects. Addition of OXFBD02 (**1a**) led to a concentration-dependent suppression of NF-κB-dependent gene expression (Fig. 3), indicating that it also disrupts the interaction of the BRD4 bromodomains with KAc310 of RelA. The fact that complete repression of NF-κB-dependent transcription was not observed with either **1a** or (+)-JQ1 suggests that there might be other PPIs involved in this process.

2.2. Designing compounds to investigate the WPF shelf-binding region

Taken together the data above indicate that the series of compounds exemplified by OXFBD02 (**1a**) are potentially useful tools to investigate the function of the BET bromodomains in cellular and ultimately *in vivo* settings. With this in mind, we used Metasite 3.1.2 (phase I) and Meteor 2.0.2 (phase I and II) to predict the metabolic liabilities of OXFBD02 (**1a**) (Fig. S3). This analysis indicated that the 4-position of the phenyl ring was the most significant liability, presumably through CYP450-catalysed oxidation. In accordance with this prediction, investigation of the metabolic stability of OXFBD02 (**1a**) in human liver microsomes showed that **1a** is a relatively high clearance compound, with CL_{int} of 34.8 μL/min/mg protein and a cellular half-life of 39.8 min (Table S2).

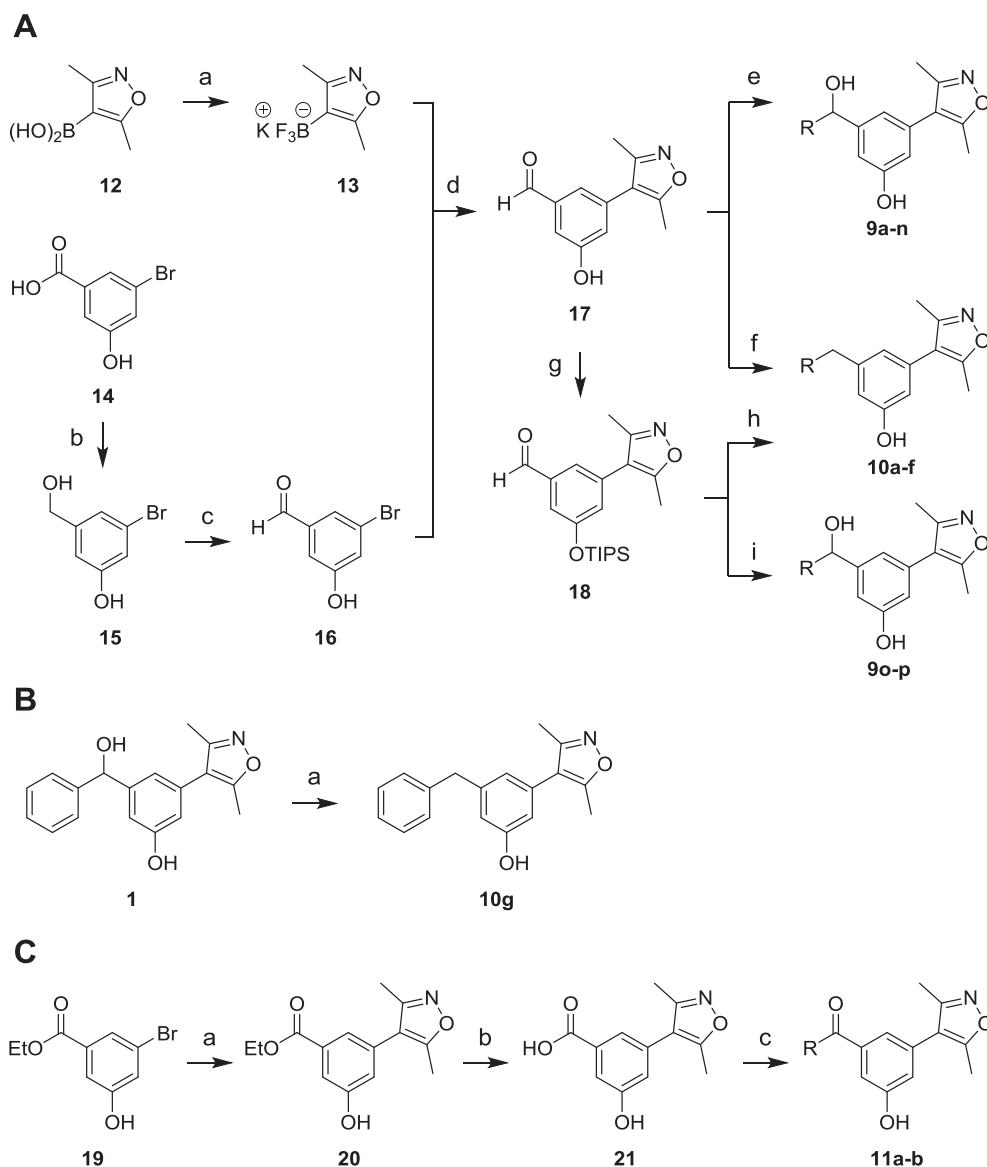
These data are consistent with work by Sharp et al. who showed that, in a direct comparison, 3,5-dimethylisoxazole-based compounds showed the highest affinity for the BET bromodomain, but also poor metabolic stability.³¹ Therefore, while optimising our compounds we wished to determine whether poor metabolic stability is an inherent problem with 3,5-dimethylisoxazole-based compounds, or whether by carefully balancing the properties of the whole molecule this apparent liability can be overcome.

Given the structure of **1a**, and the metabolic liability of the *para*-position, the region of the molecule that is most suitable for optimisation is the WPF shelf-binding phenyl ring. It has generally been observed that binding of a lipophilic moiety to this region confers high affinity for the BET bromodomains.⁷ However, the lipophilicity of this group has to be balanced with the overall properties of the molecule to ensure that the compound is soluble. Solubility Forecast Index ($SFI = clogD_{pH7.4} + \#Ar$)⁴⁵ is a useful parameter for predicting compound solubility, and is especially useful for comparing molecules within a series. OXFBD02 (**1a**) is soluble enough to be used in *in vitro* and cellular settings, and has $SFI = 6.6$, suggesting that new analogues should have an SFI value of 6.6 or lower to ensure useful solubility. In addition, CL_{int} is hydrophobicity dependent and therefore reducing compound hydrophobicity might help to improve compound metabolic stability.⁴⁶ Based on these observations, and cognisant of work by Gehling et al.³⁰ we designed a series of compounds to probe the WPF shelf-binding region of the molecule. In particular we wished to explore blocking the 4-position of the phenyl ring with metabolically stable functionality to be a facile way to overcome the issue of metabolic oxidation.

Compounds with both electron-withdrawing and electron-donating substituents at the 2-, 3-, and 4-position of the ring (**9a–e**, **g**, **l**, **m**, **o**) were designed to probe the optimum electronics and vector for ring substitution. Compound **9f** contains 3,4-dichloro-substitution to determine whether two substituents are tolerated on the phenyl ring. The 2-, 3-, and 4-pyridyl derivatives (**9j**, **k**, **p**) were designed as these compounds have favourable SFI values of 5.9, and the 4-chloro-2-pyridyl derivative (**9n**) was designed to reduce the basicity of the pyridine nitrogen atom ($pK_a = 2.22$ (pK_a value of the conjugated acid), predicted using ACD/Labs I-Lab 2.0 software [Algorithm Version: v12.1.0.50374]). We designed compounds with cyclohexyl and cyclopropyl substituents (**9h–i**) to determine whether non-aromatic rings are accepted by the WPF shelf. We also wished to probe whether the secondary hydroxyl group is essential for good BET bromodomain affinity, and so a series of compounds was designed without this functionality, which also allowed the introduction of less polar solubilising groups, mainly *via* reductive amination. In this series, we investigated whether more polar groups, conveying favourable physicochemical properties to the molecule (**10a–g**), are able to bind the WPF shelf. We were particularly interested in 4,4-difluoropiperidinyl analogue (**10d**) as the two geminal fluorine substituents were predicted to lower basicity of the tertiary amine ($pK_a = 4.67$ (conjugated acid of the tertiary amine)), predicted using ACD/Labs I-Lab 2.0 software [Algorithm Version: v12.1.0.50374], Table S3), which suggests that the compound will exist in a predominantly deprotonated state at physiological pH, allowing binding of the WPF shelf. We also designed two amide-based compounds (**11a–b**) to investigate the importance of the tetrahedral carbon atom proximal to the WPF shelf-binding group.

2.3. Synthesis

Our general synthetic strategy is based on that previously reported for the OXFBD02 (**1a**).²¹ The synthesis of aldehyde **17** has been optimised (Scheme 1A and Supporting Information) as this is a key intermediate in the synthesis of the secondary alcohols



Scheme 1. Synthesis of the 3,5-dimethylisoxazole-based compounds **9–11**. (A) Synthesis of the secondary alcohols **9a–p** (**9a**: R = 4-chlorophenyl, **9b**: R = 2-methoxyphenyl; **9c**: R = 3-methoxyphenyl; **9d**: R = 4-methoxyphenyl; **9e**: R = 4-tolyl; **9f**: R = 3,4-dichlorophenyl; **9g**: R = 4-fluorophenyl; **9h**: R = cyclohexyl; **9i**: R = cyclopropyl; **9j**: R = 3-pyridyl; **9k**: R = 4-pyridyl; **9l**: R = 3-fluorophenyl; **9m**: R = 4-cyanophenyl; **9n**: R = 4-chloro-2-pyridyl, **9o**: R = 2-fluorophenyl, **9p**: R = 2-pyridyl) and the amines **10a–f** (**10a**: R = N-methylpiperazinyl; **10b**: R = morpholinyl; **10c**: R = N-benzylamino; **10d**: R = 4,4-difluoropiperidinyl; **10e**: R = piperidinyl; **10f**: R = pyrrolidinyl). *Reagents and conditions*: (a) KF, L-(+)-tartaric acid, CH₃CN/THF, rt, 30 min, 59–73% (n = 2); (b) BH₃·THF, THF, 0 °C then rt, 18 h, 80–96% (n = 3); (c) MnO₂, CHCl₃/EtOAc, reflux, 2 h, 49–78% (n = 3); (d) Pd(OAc)₂, RuPhos, Na₂CO₃, EtOH, 80 °C, 85%; (e) for **9a–e**: RMgBr, THF, rt, 3–19 h, 51–80%; for **9f**: 3,4-dichlorophenylmagnesium bromide, THF, 50 °C, 14 h, 11%; for **9g–i**: Aryl/alkyl bromide, Mg, I₂, THF, rt to reflux, 30–60 min, then **17**, THF, 0 °C to rt, 2–18 h, 72–85%; for **9j**: 3-bromopyridine, isopropylmagnesium chloride lithium chloride complex, THF, rt, 2 h, then **17**, THF, rt, 4 h, 73%; for **9k**: 4-iodopyridine, isopropylmagnesium chloride, THF, rt, 1 h, then **17**, THF, rt to 50 °C, 22 h, 9%; for **9l–n**: Aryl iodide, isopropylmagnesium chloride lithium chloride complex, THF, –10 °C to rt, 2–5 h, then **17**, THF, rt to 50 °C, 3 h to 2 d, 11–23%; (f) for **10a–c**: amine, AcOH, EtOH, pH = 4, rt, 20–40 min, then NaBH₃CN, rt, 17–23 h, 20–69%; for **10d**: 4,4-difluoropiperidine hydrochloride, EtOH, rt, 30 min, then NaBH₃CN, rt, 19 h, 33%; (g) TIPSCl, imidazole, DMF, 0 °C to rt, 13 h, 84%; (h) Amine, AcOH, EtOH, rt, 1 h, then NaBH₃CN, rt, 22 h, then TBAF, THF, 0 °C to rt, 1–2 h, 8–33%; (i) Aryl bromide, ^tBuLi, THF, –78 °C, 40 min, then **18**, THF, –78 °C to rt, 3–16 h, then TBAF, THF, 0 °C, 0.5–2 h, 17–89%; (B) Synthesis of **10g**. *Reagents and conditions*: (a) Et₃SiH, TFA, rt, 15 min, 70%; (C) Synthesis of **11a–b**. *Reagents and conditions*: (a) **13**, Pd(OAc)₂, RuPhos, Na₂CO₃, EtOH, 90 °C, mw, 1.5 h, 68%; (b) LiOH, THF, rt, 24 h, 96%; (c) EDC hydrochloride, HOBt hydrate, THF, rt, 20 min, then amine, 55 °C, 3 d, 52–56% (see Experimental Section for more detailed procedures).

9a–n, and the amines **10a–d**. The secondary alcohols **9o–p** were generated by reaction of the TIPS-protected analogue **18** with organolithium reagents (Scheme 1A), followed by deprotection.

Reductive amination of **18** with subsequent deprotection furnished the amines **10e–f** (Scheme 1A). The methylene derivative **10g** was synthesised by treating OXFBD02 (**1a**) with TFA and Et₃SiH to reduce the secondary alcohol (Scheme 1B). To obtain the amides **11a–b** we coupled the carboxylic acid **21** to the appropriate secondary amine using 1-ethyl-3-(3-dimethylaminopropyl)carbodiimide (EDC) (Scheme 1C). Detailed information for the synthe-

sis of all final compounds (**9a–p**, **10a–f**, **11a–b**) as well as the intermediates (**13**, **15–18**, **20–21**) can be found in the Experimental Section.

2.4. In vitro inhibition and SAR studies

A well-validated Amplified Luminescence Proximity Homogeneous Assay (AlphaScreen™) peptide displacement assay was used to measure the BRD4(1) IC₅₀ values for the synthesised compound, and the data obtained are shown in Table 1.⁴⁷

Addition of a 4-chloro substituent (**9a**, Table 1) resulted in a small drop in BRD4(1) affinity ($IC_{50} = 0.631 \mu\text{M}$). Addition of a methoxy group was generally well tolerated, with 2-position (**9b**) substitution preferred ($IC_{50} = 0.270 \mu\text{M}$) over 3- (**9c**) or 4-position (**9d**) substitution. The 4-tolyl derivative (**9e**) showed similar affinity to **1a**, indicating that lipophilic substituents are favourable for BRD4(1) binding. Interestingly, fluorine was less well tolerated than other substituents (**9g**, **1**, **o**), with the 2-fluoro derivative (**9o**) displaying the lowest BRD4(1) affinity ($IC_{50} = 1.42 \mu\text{M}$). The 3-pyridyl (**9j**, $IC_{50} = 0.166 \mu\text{M}$) and 4-pyridyl (**9k**, $IC_{50} = 0.303 \mu\text{M}$) derivatives showed high BRD4(1) affinity. Intriguingly the 2-pyridyl derivative (**9p**) showed substantially reduced BRD4(1) affinity ($IC_{50} = 4.68 \mu\text{M}$). Both the cyclopropyl (**9i**) and cyclohexyl substituents (**9h**) were well tolerated. The cyclohexyl derivative displayed the joint highest affinity ($IC_{50} = 0.166 \mu\text{M}$) for BRD4(1), albeit at the expense of increased lipophilicity ($\text{clogD}_{7.4} = 4.24$, $\text{LLE} = 3.54$) compared to the equipotent 3-pyridyl derivative (**9j**, $\text{clogD}_{7.4} = 2.96$, $\text{LLE} = 5.74$). The phenyl derivative in which the secondary hydroxyl group is removed (**10g**) showed a significantly reduced BRD4(1) affinity ($IC_{50} = 1.10 \mu\text{M}$) compared to the matched pair of compound **1a**. In general, other more polar substituents were poorly tolerated and displayed higher IC_{50} values. The piperazine amide derivative (**11a**) was relatively well tolerated, whereas the morpholine derivative (**11b**) was not.

We determined a BRD4(1) dissociation constant (K_d) for **9j** of $0.247 \mu\text{M} \pm 0.08 \mu\text{M}$ using isothermal titration calorimetry (ITC) (Fig. S4A), which is consistent with the AlphaScreen results. For **1a** we determined a K_d value of $0.435 \mu\text{M} \pm 0.16 \mu\text{M}$ (Fig. S4B). Selectivity profiling in a BROMOScan assay against 12 phylogenetically diverse bromodomains confirmed that both **1a** and **9j** potent BET bromodomain ligands, with additional modest affinity for the CREBBP bromodomain, but no significant affinity for any of the other of the selected bromodomains investigated (Table S4).

2.5. Structural studies

To understand the structural basis of our SAR observations we obtained X-ray crystal structures of the 3-pyridyl derivative (**9j**; PDB code 6FSY), the cyclopropyl derivative (**9i**; PDB code 6FT3), and the difluorinated piperidine derivative (**10d**; PDB code 6FT4) in complex with BRD4(1). In all cases the molecules bind to BRD4(1) broadly as expected. The 3,5-dimethylisoxazole acts as the KAc mimic and forms a hydrogen bond with N140 and a water-mediated hydrogen bond with Y97 (Fig. 4A). Interestingly in the case of **9j** and **9i**, only the (*R*)-enantiomer is observed in the X-ray crystal structure, despite a racemate being submitted to crystallisation. It should be noted that despite these two molecules having the same absolute configuration, they have the opposite sense of stereochemistry due to the priority assignment of the pyridine ring compared to the cyclopropyl ring.

Compound **9j** overlays precisely with (*S*)-OXFBD02 (which has the same sense of stereochemistry; PDB code 4J0S) with the pyridine ring occupying the WPF shelf (Fig. 4B). The pyridine nitrogen is oriented away from the W81 and forms a water-mediated hydrogen bond with D145. It is feasible that this additional interaction, which is not present in OXFBD02, is responsible (at least in part) for the increase in BRD4(1) affinity displayed by **9j**. Interestingly, the pyridine nitrogen does not overlay with that of I-BET151 (**3**) when bound to BRD4(1) (PDB code 3ZYU) (Fig. 4C), and the nitrogen atom in I-BET151 does not appear to form any interactions with BRD4(1). The phenol moiety of **9j** forms a hydrogen bond to the ZA-channel water molecule in the same manner as OXFBD02 (**1a**). The cyclopropyl derivative (**9i**) does not overlay so precisely with (*R*)-OXFBD02, with the hydroxyl group oxygen atoms displaced by 1.4 \AA . The cyclopropyl group occupies the WPF shelf and is oriented towards W81. However, analysis of the

B-factors for the ligand indicates that the cyclopropyl ring is the most flexible component of the molecule, and that in general **9i** is more flexible than **9j**, perhaps reflecting the higher affinity of the latter for BRD4(1).

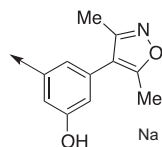
The SAR of the pyridyl derivatives (**9j**, **k**, **p**) is particularly intriguing given the significant difference in BRD4(1) resulting from moving the nitrogen atom one position around the ring. We hypothesised that the decreased potency of 2-pyridyl derivative **9p** could be affected by the formation of an intramolecular H-bond between the nitrogen lone pair of the 2-pyridyl substituent and the secondary hydroxyl group. This interaction cannot form in the 3-pyridyl derivative **9j**. We conducted ^1H NMR experiments to determine whether we could detect formation of an internal hydrogen bond in **9p** in solution. To assess the presence and strength of a solution-phase hydrogen bond we observed the change in chemical shift of the given hydrogen atom when the ^1H NMR solvent is changed from CDCl_3 to D_6 -DMSO.⁴⁸ The chemical shift of hydrogen atoms that are not engaged in hydrogen bonds typically show a $\Delta_{\text{ppm}} \text{CDCl}_3 \rightarrow \text{D}_6\text{-DMSO} = 2\text{--}4 \text{ ppm}$, as their environment is predominantly dictated by the surrounding solvent. Hydrogen atoms that are involved in a hydrogen bond typically show $\Delta_{\text{ppm}} \text{CDCl}_3 \rightarrow \text{D}_6\text{-DMSO} < 1 \text{ ppm}$, as their environment is mainly dictated by the intramolecular interaction, and hence less affected by the surrounding solvent. This technique is especially powerful when combined with structural studies, as it allows comparison between intramolecular hydrogen bonds formed in solution phase and those present when a ligand is bound to a protein.

In D_6 -DMSO, the signal for the phenolic hydroxyl group of **9p** shifts downfield ($\Delta_{\text{ppm}} \text{CDCl}_3 \rightarrow \text{D}_6\text{-DMSO} = +4.2 \text{ ppm}$) consistent with this group being solvent exposed. In contrast, only a small change was seen for the secondary alcohol ($\Delta_{\text{ppm}} \text{CDCl}_3 \rightarrow \text{D}_6\text{-DMSO} = +0.8 \text{ ppm}$), which supports the idea that this group is engaged in an intramolecular hydrogen bond (Fig. 5A). We hypothesised that the 4-chloro-2-pyridyl derivative (**9n**) would have a less basic nitrogen atom due to the inductive electron withdrawing effects of the 4-chloro substituent, and that this would result in a weaker internal H-bond. Consistent with this prediction, we observed an increased $\Delta_{\text{ppm}} \text{CDCl}_3 \rightarrow \text{D}_6\text{-DMSO}$ of $+1.6 \text{ ppm}$ for the secondary alcohol, indicating a weaker internal hydrogen bond ($\Delta_{\text{ppm}} \text{CDCl}_3 \rightarrow \text{D}_6\text{-DMSO} = +4.7 \text{ ppm}$ for the phenol of **9n**). This compound shows intermediate BRD4(1) affinity ($IC_{50} = 495 \text{ nM}$) between **9j** and **9p**.

We proposed that the internal hydrogen bond present in **9p** would result in the molecule adopting a solution state conformation that was unfavourable for protein binding. To investigate this idea, we conducted molecular dynamics (MD) simulations to predict the conformation that both enantiomers of **9p** would adopt when bound to BRD4(1). A 50 ns simulation indicates that (*S*)-**9p** adopts a very similar conformation to (*R*)-OXBDF02, and that in this conformation the internal hydrogen bond is intact (Fig. 6A). In this conformation the pyridine nitrogen atom is facing towards the solvent and away from W81, which is also the case in the X-ray crystal structure of **9j**, and an X-ray crystal structure of I-BET151 (**3**) which contains a 2-pyridyl substituent (Fig. 4C).

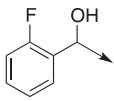
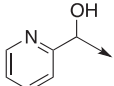
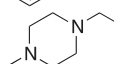
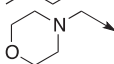
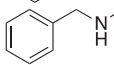
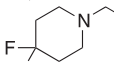
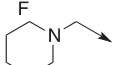
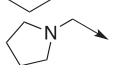
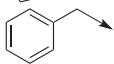
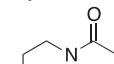
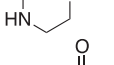
We reasoned that the orientation of the nitrogen atom away from the hydrophobic W81 residue is likely favourable. However, while the (*S*)-enantiomer of **9p** can adopt this orientation and maintain the internal hydrogen bond, the (*R*)-enantiomer would not be able to bind to BRD4(1) and maintain the internal hydrogen bond. This was shown to be the case in a 50 ns MD simulation, where the pyridine nitrogen is oriented away from W81, and consequently the internal hydrogen bond is broken (Fig. 6B). This observation provides an explanation for the low BRD4(1) affinity displayed by racemic **9p**, as only half the concentration of the ligand can bind to BRD4(1) with the internal hydrogen bond intact. In the opposite enantiomer a large enthalpic penalty to break the

Table 1
 IC₅₀ values, pIC₅₀ values, ligand efficiencies (LE), clogP values, lipophilic ligand efficiencies (LLE), cLogD_{PH7.4} values, and solubility forecast index (SFI) for **9a-p**, **10a-g**, **11a-b**, including **1a** as a reference compound. Heat map shows relative IC₅₀ values obtained in an AlphaScreen assay.⁴⁷ Red indicates low IC₅₀ values, and green indicates high IC₅₀ values. Quoted IC₅₀ values are a mean of three technical repeats. Ranges in parentheses represent 95% confidence intervals resulting from sigmoidal curve fitting to the triplicate data.



Compound	Substituent	BRD4(1) IC ₅₀ (μM) ^a	pIC ₅₀	LE	cLogP ^b	LLE	cLogD _{PH7.4} ^b	SFI
1a		0.384 (0.346–0.420) ^c	6.42	0.41	2.53	3.89	3.62	6.62
9a		0.631 (0.539–0.739)	6.20	0.38	3.13	3.07	4.28	7.28
9b		0.270 (0.223–0.327)	6.57	0.38	2.45	4.12	3.80	6.80
9c		0.478 (0.402–0.570)	6.32	0.37	2.45	3.87	3.80	6.80
9d		0.585 (0.531–0.644)	6.23	0.36	2.45	3.78	3.80	6.80
9e		0.296 (0.264–0.332)	6.53	0.40	2.99	3.54	4.32	7.32
9f		0.945 (0.865–1.03)	6.02	0.35	3.60	2.42	5.01	8.01
9g		0.842 (0.697–1.02)	6.07	0.37	2.59	3.48	4.00	7.00
9h		0.166 (0.158–0.175)	6.78	0.43	3.24	3.54	4.24	6.24
9i		0.377 (0.339–0.420)	6.42	0.47	1.54	4.88	3.26	5.26
9j		0.166 (0.142–0.193)	6.78	0.43	1.04	5.74	2.96	5.96
9k		0.303 (0.262–0.349)	6.52	0.41	1.04	5.48	2.86	5.86
9l		0.793 (0.685–0.919)	6.10	0.37	2.59	3.51	4.00	7.00
9m		0.604 (0.536–0.680)	6.22	0.36	1.97	4.25	3.53	6.53
9n		0.495 (0.427–0.574)	6.31	0.38	1.89	4.42	3.49	6.49

Table 1 (continued)

Compound	Substituent	BRD4(1) IC ₅₀ (μM) ^a	pIC ₅₀	LE	cLogP ^b	LLE	cLogD _{pH7.4} ^b	SFI
9o		1.42 (1.21–1.68)	5.85	0.36	2.59	3.26	4.00	7.00
9p		4.68 (3.40–6.45)	5.33	0.34	1.04	4.29	2.96	5.96
10a		1.23 (1.02–1.47)	5.91	0.38	0.72	5.19	1.41	3.41
10b		0.956 (0.802–1.14)	6.02	0.40	0.97	5.05	2.34	4.34
10c		2.25 (1.82–2.77)	5.65	0.34	3.21	2.44	2.34	5.34
10d		0.235 (0.210–0.263)	6.63	0.40	1.37	5.26	3.62	5.62
10e		4.28 (3.39–5.40)	5.37	0.36	2.55	2.82	2.22	4.22
10f		3.27 (2.43–4.38)	5.49	0.38	1.98	3.51	1.27	3.27
10g		1.10 (0.990–1.22)	5.96	0.40	4.00	1.96	4.96	7.96
11a		0.722 (0.568–0.918)	6.14	0.39	1.62	4.52	3.21	5.21
11b		3.80 (3.04–4.74)	5.42	0.34	0.07	5.35	2.38	4.38

^a Protein concentration was adjusted to a final assay concentration of 10 nM, peptide concentration was 4 nM (see Supporting Information for detailed assay procedures).

^b cLogP and cLogD_{pH7.4} values were calculated using ACD/Labs I-Lab 2.0 software (Algorithm Version: 5.0.0.184).

^c Values taken from Hewings et al.²¹

hydrogen bond must first be overcome before the ligand can bind to BRD4(1). This observation predicts that (*S*)-**9p** should have a much higher affinity for BRD4(1) than (*R*)-**9p**. Work to investigate this is ongoing but is beyond the scope of these studies.

Compounds **10a–f** were designed to investigate whether more polar groups would be tolerated on the WPF shelf. As might be expected, most of these compounds show low BRD4(1) affinity, in line with the idea that a lipophilic group is preferred in this region. The notable exception in this series is the geminal difluorinated piperidine (**10d**), which has an IC₅₀ value of 235 nM for BRD4(1). We attribute this to the electron-withdrawing effects of the fluorine atoms resulting in reduced basicity that suppresses amine protonation, allowing the piperidine to interact better with the lipophilic WPF shelf. An X-ray crystal structure of **10d** bound to BRD4(1) (PDB code 6FT4; Fig. 7A) confirms that the difluoropiperidine moiety does reside on the WPF shelf, as predicted. We calculated the pK_a values of the amine analogues (Table S3) and plotted the predicted appearance of the non-ionic state under assay conditions against the detected IC₅₀ values (Fig. 7B). These data suggest that positively charged amines do not bind well to the WPF shelf, with a correlation (linear regression R² = 0.8162) between BRD4(1) affinity and the pK_a of the conjugated acid of the tertiary amine observed.

While the cyclopropyl-derived **9i** shows the highest LE of the series, the 3-pyridyl derivative **9j** and the cyclohexyl analogue **9h** have the highest BRD4(1) affinity. However, while **9h** has a LLE of 3.54, **9j** shows a LLE of 5.74, indicating that this BRD4(1) ligand has an optimised balance of affinity and physicochemical properties.

2.6. Metabolism and cellular studies

The metabolic stability of our most promising compounds (**9j**, **10d**) was tested in a human microsomal stability assay using OXFBD02 (**1a**) as a reference. The cyclohexyl derivative **9h** was excluded from these studies as its more lipophilic nature limits its solubility and increases the likelihood of a poor metabolic profile. OXFBD02 (**1a**) and the 4,4-difluoropiperidinyl derivative (**10d**) exhibited similar metabolic half-lives, with t_{1/2} = 39.8 min and t_{1/2} = 27.0 min, respectively. Compounds **1a** and **10d** displayed CL_{int} values of 34.8 and 51.4 μL/min/mg protein and are consequently considered to be medium and high clearance compounds, respectively.⁴⁹ In contrast, the 3-pyridyl analogue (**9j**) displayed a significantly longer metabolic half-life of 388 min (Table 2). With an intrinsic clearance (CL_{int}) of 3.57 μL/min/mg protein, **9j** is therefore classified as a low clearance compound. These properties indicate that **9j** is the optimal ligand in this series for progression to use in cellular and potentially *in vivo* studies. However, it should be noted that the microsomal stability assay only provides insights into phase I metabolism. More comprehensive metabolic characterisation, including phase II conjugation reactions, will be included in future studies.

To rationalise the selection of compounds used for further cellular studies we have predicted the cell permeability of all final compounds presented herein. All compounds were predicted to have an absorption rate constant (K_a) between 0.053 and 0.058 min⁻¹ which suggests excellent cellular uptake (Table S5). As there is no significant difference in permeability among the synthesised compounds we decided to further study the compound **9j** displaying

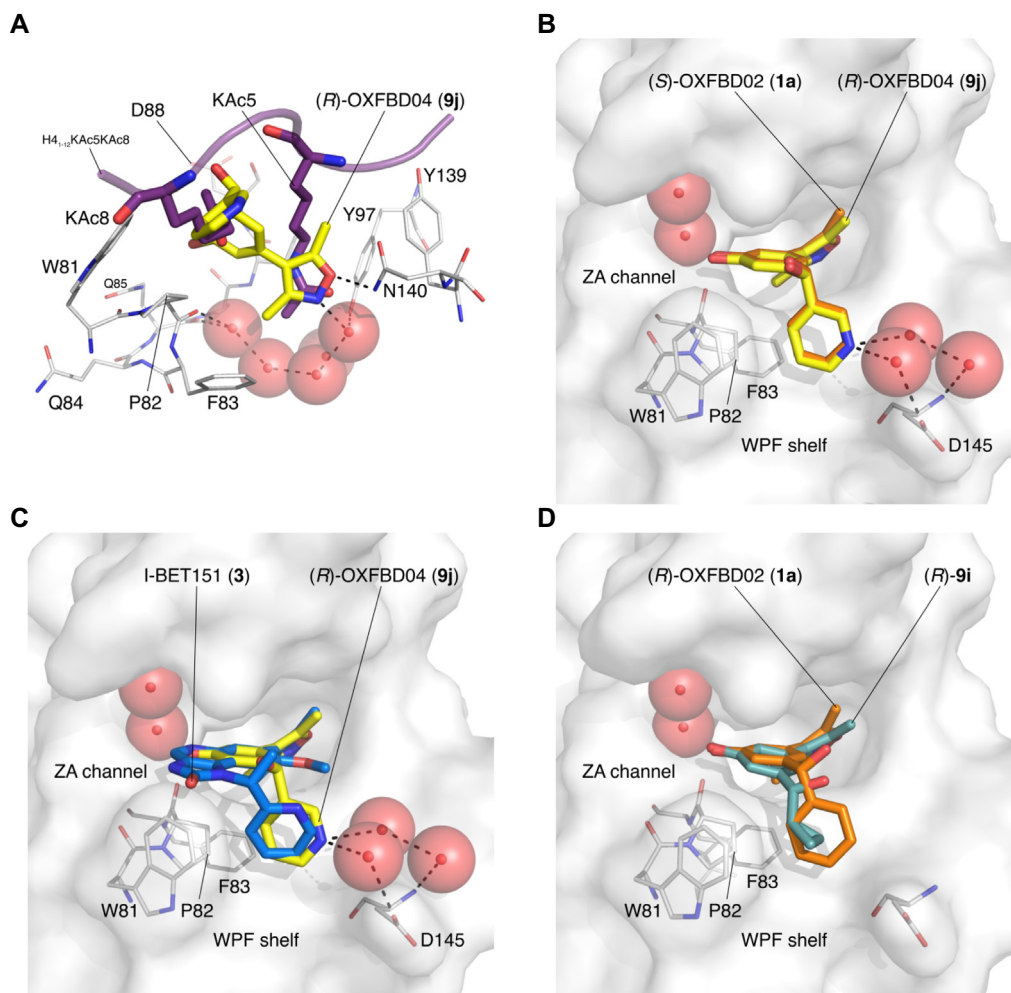


Fig. 4A. Overlaid X-ray crystal structures of (*R*)-OXFBD04 [(*R*)-**9j**, PDB code **6FSY**, carbon = yellow; resolution: 1.34 Å] and the diacetylated histone H4-mimicking peptide H4₁₋₁₂KAc5KAc8 (PDB code **3UVW**, carbon = purple) bound to BRD4(1). **B.** Overlaid X-ray crystal structures of (*R*)-OXFBD04 [(*R*)-**9j**, PDB code **6FSY**, carbon = yellow] and (*S*)-OXFBD02 [(*S*)-**1a**, PDB code **4JOS**, carbon = orange] bound to BRD4(1), showing that the molecules have very similar binding modes to BRD4(1). (*R*)-**9j** forms additional water-mediated interactions with D145, which are not possible for **1a**. **C.** Overlaid X-ray crystal structures of (*R*)-OXFBD04 [(*R*)-**9j**, PDB code **6FSY**, carbon = yellow] and the I-BET151 (**3**, PDB code **3ZYU**, carbon = marine blue) bound to BRD4(1), showing that the pyridine nitrogen does not overlay with that of I-BET151. **D.** Overlaid X-ray crystal structures of the cyclopropyl derivative (*R*)-**9i** (PDB code **6FT3**, carbon = light teal; 1.28 Å) and (*R*)-OXFBD02 (**1a**, PDB code **4JOS**, carbon = orange) bound to BRD4(1), showing that the molecules do not overlay precisely when binding to BRD4(1). (For interpretation of the references to colour in this figure legend, the reader is referred to the web version of this article.)

to most promising results in our previous studies in a cellular setup. In a cell growth assay using A498 (renal), HT-29 (colon), and MCF7 (breast) cancer cell lines, **9j** showed low micromolar activity (Table 3 and Fig. S11). OXFBD02 was used as a positive control, and the data for OXFBD02 are in line with that obtained in the NCI-60 screen. To address the mechanism of cytotoxicity, we probed the effect of **9j** and **1a** on *MYC* suppression in MCF7 cells. We show that **9j** exerts a potent and time-dependent effect of *MYC* suppression similar to **1a** and (+)-JQ1, which was used as a positive control (Fig. 8). These data indicate that OXFBD04 (**9j**) shows similar cellular efficacy to OXFBD02 (**1a**), which combined with its enhanced metabolic stability makes OXFBD04 (**9j**) a useful tool compound for studying the function of the BET bromodomains.

3. Conclusion

In conclusion, we have shown that the BET bromodomain ligand OXFBD02 (**1a**) displays a promising profile in the NCI-60 panel of

cancer cell lines, but a short metabolic half-life of 40 min in human liver microsomes. To optimise the metabolic stability of this compound series, we investigated the SAR of WPF-binding groups, with a view to optimising the overall compound properties. In the pyridyl series we showed that an intramolecular hydrogen bond detrimentally affects the affinity of 2-pyridyl derivative (**9p**), by holding the (*R*)-enantiomer in a conformation that disfavors BRD4(1) binding. However, the 3-pyridyl derivative, OXFBD04 (**9j**), displays higher BRD4(1) affinity than the parent compound and an LLE value of 5.74, indicating that it is a BRD4(1) ligand with an optimised balance of affinity and physicochemical properties. The addition of the pyridine ring led to an increased metabolic half-life of 6.5 h in human liver microsomes. These data indicate that the 3,5-dimethylisoxazole group is not inherently metabolically labile, and optimisation of the overall compound properties can lead to compounds with useful metabolic stabilities. In cancer cell lines, OXFBD04 (**9j**) showed similar effects on cytotoxicity and *MYC* suppression compared to the parent compound OXFBD02 (**1a**).

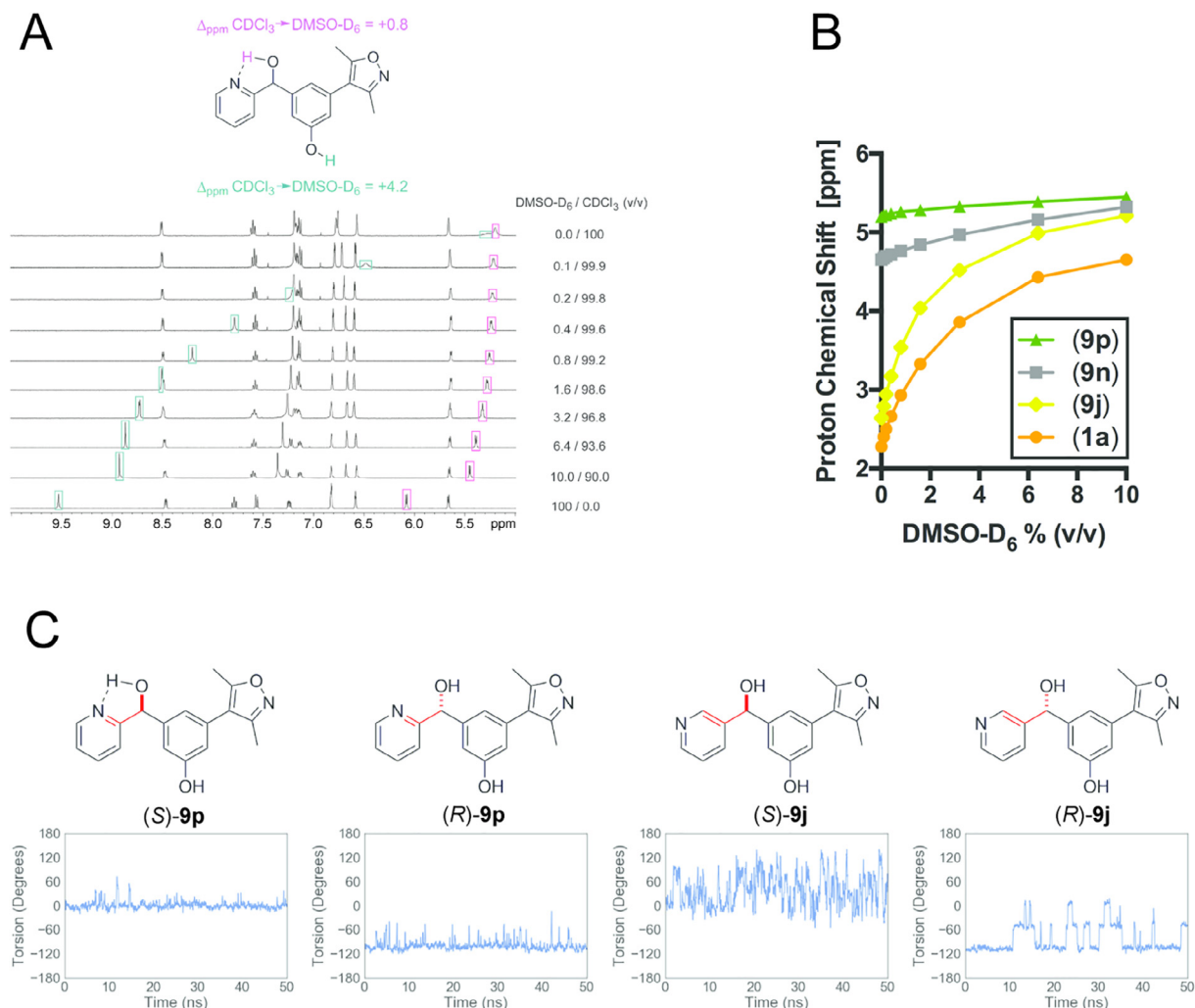


Fig. 5. Studies to rationalise the observed structure–activity relationship. A) ¹H NMR spectra of **9p** dissolved in different mixtures of CDCl₃ and D₆-DMSO displayed in a range from 5.0 to 10.0 ppm. (B) Chemical shifts of –CHOH protons of pyridyl analogues **9p**, **9n**, **9j**, and **1a**, which was used as a control for a compound that is not able to form an intramolecular H-bond, plotted against D₆-DMSO concentration. All experiments were performed at a compound concentration of 2 mg/mL. See Figure S5–8 for additional information. (C) Molecular dynamics studies for the enantiomers of **9p** and **9j** bound to BRD4(1). Representative plots showing the moving average of the dihedral angle between the bonds shown in red during three 50 ns MD simulations. A graph summarising the results of all randomised MD simulations that have been performed can be found in Figure S9–10. (For interpretation of the references to colour in this figure legend, the reader is referred to the web version of this article.)

Consequently, we report OXFDB04 (**9j**) as an improved tool compound to study BRD4 in *in vitro* and potentially *in vivo* settings.

4. Experimental

4.1. General chemistry experimental details

¹H NMR spectra were recorded on Bruker AVIII HD 400 (400 MHz) or Bruker AVII 500 (500 MHz). Chemical shifts are reported as δ_{H} part per million (ppm) relative to the solvent reference peak as internal deuterium lock.⁵⁰ The multiplicity of each signal is indicated by: s (singlet), d (doublet), t (triplet), dd (doublet of doublets), q (quartet), sp (septet) or m (multiplet). Identical proton coupling constants (*J*) are averaged in each spectrum and are reported to the nearest 0.1 Hz. Coupling constants were determined using Bruker TopSpin software. ¹³C NMR spectra were recorded on Bruker AVIII HD 400 (101 MHz) or Bruker AVII 500 (126 MHz). Chemical shifts are reported as δ_{C} part per million (ppm) relative to the solvent reference peak as internal deuterium lock. Coupling constants (*J*) are quoted in Hz and are recorded to the nearest 1 Hz. Identical coupling constants (*J*) are averaged in

each spectrum and reported to the nearest 1 Hz. The coupling constants are determined by analysis using Bruker TopSpin software. ¹⁹F NMR spectra were recorded on a Bruker AVII 500 (470 MHz) using a broadband proton decoupling pulse sequence and deuterium internal lock. The chemical shift data for each signal are given as δ_{F} in units of parts per million (ppm). ¹¹B NMR spectra were recorded on a Bruker DRX500 (160 MHz). The chemical shift data for each signal are given as δ_{B} in units of parts per million (ppm). Coupling constants (*J*) are quoted in Hz and are recorded to the nearest 1 Hz. Identical coupling constants (*J*) are averaged in each spectrum and reported to the nearest 1 Hz. The coupling constants are determined by analysis using Bruker TopSpin software. Note: in all isoxazole-containing compounds, positions on the central aromatic ring are numbered first, the isoxazole ring with primes (') and any additional rings with double primes (') etc. Low-resolution mass spectra (LRMS) using electron spray ionisation were recorded on a Micromass LCT Premier spectrometer. Electrospray Ionisation (ESI) High-Resolution Mass Spectrometry (HRMS) spectra were acquired on either a Bruker MicroTOF spectrometer or a Thermo Exactive mass spectrometer, equipped with Agilent 1100 liquid chromatography systems for flow injection

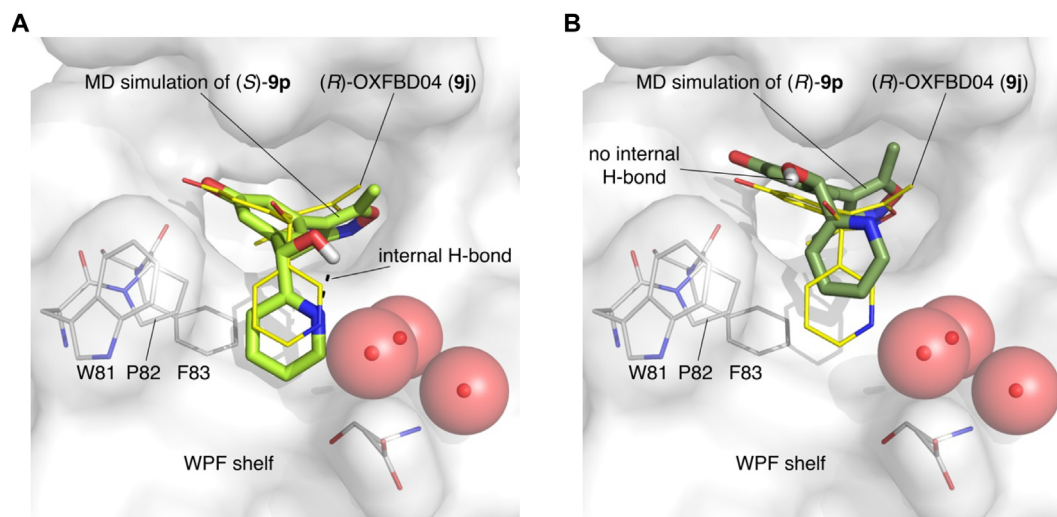


Fig. 6A. A representative image of a 45 ns MD simulation of (*S*)-**9p** overlaid with the X-ray crystal structures of (*R*)-OXFBD04 [(*R*)-**9j**, PDB code 6FSY, carbon = yellow] bound to BRD4(1). The predicted internal hydrogen-bond is present in (*S*)-**9p**. **B.** A representative image of a 50 ns MD simulation of (*R*)-**9p** overlaid with the X-ray crystal structures of (*R*)-OXFBD04 [(*R*)-**9j**, PDB code 6FSY, carbon = yellow] bound to BRD4(1). The simulation indicates that it is favourable for the pyridine nitrogen atom of (*S*)-**9p** to orient away from W8, requiring the internal hydrogen bond to be broken. (For interpretation of the references to colour in this figure legend, the reader is referred to the web version of this article.)

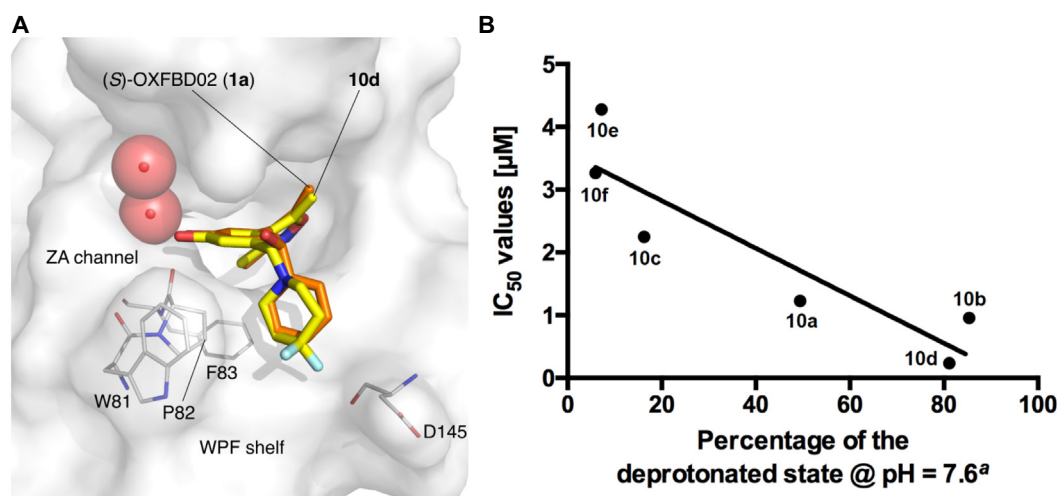


Fig. 7A. Overlaid X-ray crystal structures of **10b** (PDB code 6FT4, carbon = yellow; resolution: 1.34 Å) and (*S*)-OXFBD02 (**1a**, PDB code 4J0S, carbon = orange)²¹ bound to BRD4(1). The inductive electron-withdrawing effect of the fluorine atoms reduces the basicity of the piperidine nitrogen sufficiently for it to remain unprotonated and bind to the WPF shelf. **B.** BRD4(1) IC_{50} values of amines (**10a-f**) plotted against the predicted appearance of the non-ionic state under assay conditions (pH = 7.6). Linear regression gives a R^2 value of 0.8162, indicating a good correlation between reduced basicity and increased BRD4(1) affinity. ^aCalculated using ACD/Labs I-Lab 2.0 software (Algorithm Version: v5.0.0.184). (For interpretation of the references to colour in this figure legend, the reader is referred to the web version of this article.)

Table 2

Metabolic stability data of **1a**, **9j**, and **10d** including the intrinsic clearance ($CL_{int} \pm$ standard error) and the apparent half-life ($t_{1/2}$) detected by means of a microsomal stability assay using human liver microsomes. Dextromethorphan and verapamil were used as medium and high clearance controls, respectively. Compounds were tested at a concentration of 3 μ M.

Compound	CL_{int} (μ L/min/mg protein)	$t_{1/2}$ (min)	n
OXFBD02 (1a)	34.8 ± 3.76	39.8	5
9j	3.57 ± 2.21	388	5
10d	51.4 ± 2.6	27.0	5
Dextromethorphan	25.4 ± 4.23	54.5	5
Verapamil	192 ± 11.3	7.20	3

analysis, from solutions of MeOH, H₂O or MeCN as stated. Micro-TOF data were processed using Bruker Hystar software, while Exactive data were analysed using Thermo Xcalibur software. Melting

Table 3

GI_{50} data for OXFBD02 (**1a**) and OXFBD04 (**9j**). A498 (renal), HT-29 (colon), and MCF7 (breast) cancer cell lines were used. Values quoted are a mean of three repeats. The standard deviation is shown.

Compound	GI_{50} (μ M) A498	GI_{50} (μ M) HT-29	GI_{50} (μ M) MCF7
OXFBD02 (1a)	1.58 ± 1.35	5.79 ± 0.84	1.25 ± 0.47
OXFBD04 (9j)	4.88 ± 1.54	4.40 ± 0.81	1.40 ± 0.60

points on crystallised samples were determined using either a) a Leica Galen III hot stage microscope or b) a Griffin capillary tube melting point apparatus and are uncorrected. The solvents of crystallisation are shown in parentheses. Infrared spectra were obtained from thin films using a diamond attenuated total reflectance module. The spectra were recorded on a Bruker Tensor 27 spectrometer. Absorption maxima (ν_{max}) are reported in

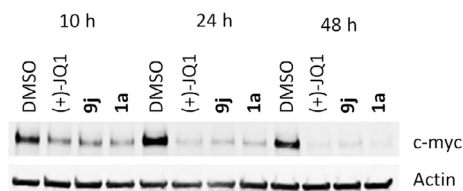


Fig. 8. Inhibition of BET bromodomains by means of 3,5-dimethylisoxazole-based ligands OXFDD02 (**1a**) or OXFBD04 (**9j**) induces MYC suppression in MCF7 breast cancer cells. Representative western blot detection of c-myc after treatment with OXFBD02 (**1a**), OXFBD04 (**9j**), or (+)-JQ1 as a reference. Compounds were tested at a concentration of 10 μ M.

wavenumbers (cm^{-1}) and are classified as broad (br), strong (s), medium (m) or weak (w). Analytical HPLC was carried out on a PerkinElmer Flexar system with a Binary LC Pump and UV/VIS LC Detector. For determination of compound purity following methods were applied. Method 1 (M1): a Dionex Acclaim[®] 120 column (C18, 5 μ m, 120 \AA , 4.6 \times 150 mm) was used and the solvents employed were A = 0.1% (v/v) solution of formic acid in 95% H₂O/5% MeCN; B = 0.1% (v/v) solution of formic acid in 95% MeCN/5% H₂O, and the gradient (A:B). A 10-min linear gradient of 0–100% B was run with a flow rate of 1 mL/min and detection at 254 nm. Samples were injected in DMSO, MeOH, DMSO/MeOH or DMSO/CHCl₃. Method 2 (M2): a Dionex Acclaim[®] 120 column (C18, 5 μ m, 120 \AA , 4.6 \times 150 mm) was used and the solvents employed were A = H₂O; B = MeCN. Linear gradient conditions (0–10 min, linear increase from 5% to 95% of B; 10–15 min, B = 95%) with a flow rate of 1.5 mL/min and detection at 254 nm. Samples were injected in DMSO, MeOH, DMSO/MeOH or DMSO/CHCl₃. Method 3 (M3): a Dionex Acclaim[®] 120 column (C18, 5 μ m, 120 \AA , 4.6 \times 150 mm) was used and the solvents employed were A = H₂O; B = MeCN. Linear gradient conditions (0–10 min, linear increase from 5% to 95% of B; 10–15 min, B = 95%) with a flow rate of 1.5 mL/min and detection at 220 nm. Samples were injected in DMSO, MeOH, DMSO/MeOH or DMSO/CHCl₃. All compounds that were subjected to biological evaluation had purity of \geq 95% determined by HPLC and LCMS analysis. Anhydrous solvents were obtained under the following conditions: anhydrous DMF, anhydrous MeOH and anhydrous EtOH were purchased from Sigma-Aldrich UK in SureSeal[™] bottles and used without further purification; anhydrous THF and CH₂Cl₂ were dried over activated 3 \AA molecular sieves under an argon or nitrogen atmosphere; where stated, THF was distilled from sodium and benzophenone and pyridine was distilled from CaH₂. Chemicals were purchased from Acros, Sigma-Aldrich, Alfa Aesar, Fisher, Apollo Scientific or Fluorochem. Where appropriate and if not stated otherwise, all non-aqueous reactions were performed in a flame-dried flask under an inert atmosphere of nitrogen or argon. MnO₂ was activated at 250 $^{\circ}$ C overnight prior to use. Organolithium reagents were titrated against diphenylacetic acid,⁵¹ and commercially-available organo-magnesium compounds were titrated against salicylaldehyde phenylhydrazine.⁵² Where stated, NEt₃ was dried with KOH and distilled onto KOH pellets. Isolute[®] SCX-2 cartridges for cation exchange were purchased from Biotage UK and were used according to manufacturers' protocols.

4.2. Synthetic procedures

4.2.1. 3-(3,5-Dimethyl-1,2-oxazol-4-yl)-5-[hydroxyl(phenyl)methyl]phenol (**1a**)²¹

Following the procedure of Hewings et al.²¹ to a solution of **17** (2.63 g, 12.1 mmol, 1.0 eq) in anhydrous THF at 0 $^{\circ}$ C was added dropwise a 1 M solution of phenylmagnesium bromide (34.0 mL,

34.0 mmol, 2.8 eq) in THF. The reaction solution was warmed to rt and stirred for 4 h. After this time, the volatile components were removed *in vacuo*. The resulting solid was crystallised from hot MeCN and the mother liquor was purified by silica gel chromatography, eluting with 1% AcOH and EtOAc in petroleum ether (gradient elution 15 \rightarrow 40%). The combined solids were crystallised from hot MeCN yielding **1a** (1.43 g, 40%) as an off-white crystalline solid: R_f (50% EtOAc/petroleum ether) 0.38; mp 187–190 $^{\circ}$ C (MeCN) [lit. mp 187–188 $^{\circ}$ C²¹]; ¹H NMR (400 MHz, D₆-acetone) δ 8.44 (1H, br s, C(1)OH), 7.49–7.43 (2H, m, C(2'')H & C(6'')H), 7.34–7.28 (2H, m, C(3'')H and C(5'')H), 7.24–7.19 (1H, m, C(4'')H), 6.94–6.91 (1H, m, C(6)H), 6.91–6.88 (1H, m, C(4)H), 6.67 (1H, dd, J = 1.9, 1.9 Hz, C(2)H), 5.83–5.79 (1H, m, CHOH), 4.90 (1H, d, J = 3.9 Hz, CHOH), 2.36 (3H, s, C(5')CH₃), 2.18 (3H, s, C(3')CH₃); LRMS *m/z* (ES⁺) 296 ([M + H]⁺, 100%). Data are in good agreement with literature values.²¹

4.2.2. 3-(3,5-Dimethyl-1,2-oxazol-4-yl)-5-[(4-chlorophenyl)(hydroxymethyl)phenol] (**9a**)

To a solution of **17** (96 mg, 442 μ mol, 1.0 eq) in anhydrous THF (2 mL) was added a 1 M solution of 4-chlorophenylmagnesium bromide (1.00 mL, 216 mg, 1.00 mmol, 2.3 eq) in Et₂O at rt, and the reaction solution was stirred for 19 h. The reaction was quenched with a saturated aqueous solution of NH₄Cl (15 mL), and the aqueous phase was extracted with EtOAc (3 \times 15 mL). The combined organic layers were washed with H₂O (45 mL), passed through an anhydrous frit and concentrated *in vacuo*. Purification by silica gel chromatography, eluting with EtOAc in cyclohexane (gradient elution 5 \rightarrow 100%) followed by mass-directed autopurification (0.1% formic acid, gradient elution MeCN/H₂O 30 \rightarrow 85%) afforded the desired product **9a** (74 mg, 51%) as a clear and colourless oil that solidified under vacuum to give a colourless amorphous solid: R_f (50% EtOAc/cyclohexane) 0.35; ν_{max} (thin film)/ cm^{-1} : 3457 (br) (O–H), 3015 (br), 2970 (w), 2949 (br); ¹H NMR (400 MHz, CD₃OD) δ 7.42–7.36 (2H, m, C(2'')H & C(6'')H), 7.34–7.28 (2H, m, C(3'')H & C(5'')H), 6.88–6.83 (1H, m, C(6)H), 6.82–6.77 (1H, m, C(4)H), 6.64 (1H, dd, J = 2.2, 1.6 Hz, C(2)H), 5.75 (1H, s, CHOH), 2.36 (3H, s, C(5')CH₃), 2.21 (3H, s, C(3')CH₃); ¹³C NMR (101 MHz, CD₃OD) δ 166.9 (C(5')), 160.0 (C(3')), 159.0 (C(1)), 148.0 (C(5)), 144.7 (C(4'')), 134.0 (C(1'')), 132.6 (C(3)), 129.4 (C(3'') & C(5'')), 129.3 (C(2'') & C(6'')), 119.7 (C(4)), 117.9 (C(4')), 115.9 (C(2)), 114.0 (C(6)), 75.9 (CHOH), 11.5 (C(5')CH₃), 10.8 (C(3')CH₃); HRMS *m/z* (ES⁺) Found: 352.0715 & 354.0698. C₁₈H₁₆ClNNaO₃⁺ requires [M(³⁵Cl)]⁺ & [M(³⁷Cl)]⁺ 352.0711 & 354.0683; LRMS *m/z* (ES⁺) 328 ([M(³⁵Cl)–H]⁺, 100%), 330 ([M(³⁷Cl)–H]⁺, 39%]; HPLC RT = 11.55 min, purity 95.5% (M1).

4.2.3. 3-(3,5-Dimethyl-1,2-oxazol-4-yl)-5-[hydroxy(2-methoxyphenyl)methyl]phenol (**9b**)

To a solution of **17** (94 mg, 433 μ mol, 1.0 eq) in anhydrous THF (2 mL) was added a 1 M solution 2-methoxyphenylmagnesium bromide (1.00 mL, 211 mg, 1.00 mmol, 2.3 eq) in THF at rt, and the reaction solution was stirred for 3 h. The reaction was quenched with a saturated aqueous solution of NH₄Cl (15 mL), and the aqueous phase was extracted with EtOAc (3 \times 15 mL). The combined organic layers were washed with H₂O (45 mL), passed through an anhydrous frit and concentrated *in vacuo*. Purification by silica gel chromatography, eluting with EtOAc in cyclohexane (gradient elution 10 \rightarrow 60%) afforded **9b** (113 mg, 80%) as a colourless solid: R_f (50% EtOAc/cyclohexane) 0.36; ν_{max} (thin film)/ cm^{-1} : 3196 (br) (O–H), 2993 (w), 2837 (w), 1642 (m) 1596 (s); mp 167–169 $^{\circ}$ C (EtOAc); ¹H NMR (400 MHz, CD₃OD) δ 7.49 (1H, dd, J = 7.5, 1.5 Hz, C(6'')H), 7.25 (1H, ddd, J = 7.8, 7.8, 1.5 Hz, C(3'')H), 7.01–6.92 (2H, m, C(4'')H & C(5'')H), 6.88–6.84 (1H, m, C(6)H), 6.80–6.76 (1H, m, C(4)H), 6.60 (1H, dd, J = 1.9, 1.9 Hz, C(2)

H), 6.12 (1H, s, CHOH), 3.81 (3H, s, OCH₃), 2.37 (3H, s, C(5')CH₃), 2.21 (3H, s, C(3')CH₃); ¹³C NMR (101 MHz, CD₃OD) δ 166.7 (C(5')), 160.0 (C(3')), 158.8 (C(1)), 157.7 (C(2'')), 148.1 (C(5)), 133.9 (C(1'')), 132.0 (C(3)), 129.5 (C(3'')), 127.9 (C(6'')), 121.6 (C(4'') or C(5'')), 119.9 (C(4)), 118.0 (C(4')), 115.4 (C(2)), 114.2 (C(6)), 111.7 (C(5'') or C(4'')), 70.5 (CHOH), 55.9 (OCH₃), 11.4 (C(5')CH₃), 10.7 (C(3')CH₃); HRMS *m/z* (ES⁺) Found: 326.1386. C₁₉H₂₀NO₄⁺ requires M⁺ 326.1387; LCMS (formic acid) RT = 0.88, [M+H]⁺ = 326; HPLC RT = 10.95 min, purity 98.0% (M1).

4.2.4. 3-(3,5-Dimethyl-1,2-oxazol-4-yl)-5-[hydroxy(3-methoxyphenyl)methyl]phenol (9c)

To a solution of **17** (103 mg, 474 μmol, 1.0 eq) in anhydrous THF (2 mL) was added a 1 M solution of 3-methoxyphenylmagnesium bromide (1.00 mL, 211 mg, 1.00 mmol, 2.1 eq) in THF at rt, and the reaction solution was stirred for 5 h. The reaction was quenched with a saturated aqueous solution of NH₄Cl (15 mL), and the aqueous phase was extracted with EtOAc (3 × 15 mL). The combined organic layers were washed with H₂O (45 mL), passed through an anhydrous frit and concentrated *in vacuo*. Purification by silica gel chromatography, eluting with EtOAc in cyclohexane (gradient elution 10 → 60%) afforded **9c** (106 mg, 68%) as a colourless solid: R_f (50% EtOAc/cyclohexane) 0.34; ν_{max} (thin film)/cm⁻¹: 3176 (br) (O–H), 2933 (w), 1640 (w), 1596 (w); mp 94–96 °C (EtOAc); ¹H NMR (400 MHz, CD₃OD) δ 7.24 (1H, dd, *J* = 7.8, 7.8 Hz, C(2'')H), 7.05–6.93 (2H, m, C(4'')H & C(5'')H or C(4'')H & C(6'')H or C(5'')H & C(6'')H), 6.89–6.84 (1H, m, C(6'')H), 6.84–6.76 (2H, m, C(4'')H & C(4'')H, C(5'')H or C(6'')H), 6.67–6.59 (1H, m, C(2'')H), 5.72 (1H, s, CHOH), 3.78 (3H, s, OCH₃), 2.73 (3H, s, C(5')CH₃), 2.22 (3H, s, C(3')CH₃); ¹³C NMR (101 MHz, CD₃OD) δ 166.8 (C(5')), 161.2 (C(3'')), 160.0 (C(3')), 158.9 (C(1)), 148.3 (C(1'')), 147.4 (C(5)), 132.4 (C(3)), 130.3 (C(2'')), 120.0 (C(4'')), C(5'') or C(6'')), 119.8 (C(4'')), C(5'') or C(6'')), 118.0 (C(4')), 115.7 (C(2)), 114.1 (C(6)), 113.7 (C(4)), 113.2 (C(4''), C(5'') or C(6'')), 76.6 (CHOH), 55.7 (OCH₃), 11.4 (C(5')CH₃), 10.7 (C(3')CH₃); HRMS *m/z* (ES⁺) Found: 326.1386. C₁₉H₂₀NO₄⁺ requires M⁺ 326.1387; LCMS (formic acid) RT = 0.87, [M + H]⁺ = 326; HPLC RT = 10.84 min, purity 98.5% (M1).

4.2.5. 3-(3,5-dimethyl-1,2-oxazol-4-yl)-5-[hydroxy(4-methoxyphenyl)methyl]phenol (9d)

To a solution of **17** (102 mg, 470 μmol, 1.0 eq) in anhydrous THF (2 mL) was added a 0.5 M solution of 4-methoxyphenylmagnesium bromide (2.00 mL, 211 mg, 1.00 mmol, 2.1 eq) in THF at rt, and the reaction solution was stirred for 3 h. The reaction was quenched with a saturated aqueous solution of NH₄Cl (15 mL), and the aqueous phase was extracted with EtOAc (3 × 15 mL). The combined organic layers were washed with H₂O (45 mL), passed through an anhydrous frit and concentrated *in vacuo*. Purification by silica gel chromatography, eluting with EtOAc in cyclohexane (gradient elution 10 → 60%) afforded **9d** (104 mg, 68%) as a clear and colourless oil. Precipitation from Et₂O and hexane afforded a colourless amorphous solid: R_f (50% EtOAc/cyclohexane) 0.44; ν_{max} (thin film)/cm⁻¹: 3016 (w) (O–H), 2970 (w), 1739 (s); ¹H NMR (400 MHz, CD₃OD) δ 7.34–7.26 (2H, m, C(3'')H & C(5'')H), 6.91–6.84 (3H, m, C(2'')H, C(6'')H & C(6'')H), 6.81–6.78 (1H, m, C(4'')H), 6.65–6.60 (1H, m, C(2'')H), 5.72 (1H, s, CHOH), 3.74 (3H, s, OCH₃), 2.35 (3H, s, C(5')CH₃), 2.20 (3H, s, C(3')CH₃); ¹³C NMR (126 MHz, CD₃OD) δ 166.8 (C(5')), 160.4 (C(4'')), 160.0 (C(3')), 158.9 (C(1)), 148.6 (C(5) or C(1'')), 137.9 (C(1'') or C(5)), 132.3 (C(3)), 129.0 (C(3'') & C(5'')), 119.6 (C(4)), 118.0 (C(4')), 115.5 (C(2)), 114.7 (C(2'') & C(6'')), 113.9 (C(6)), 76.2 (CHOH), 55.7 (OCH₃), 11.4 (C(5')CH₃), 10.7 (C(3')CH₃); HRMS *m/z* (ES⁻) Found: 324.1243. C₁₉H₁₈NO₄⁻ requires M⁻, 324.1241; LRMS *m/z* (ES⁻) 324 ([M–H]⁻, 100%); HPLC RT = 10.74 min, purity 97.1% (M1).

4.2.6. 3-(3,5-dimethyl-1,2-oxazol-4-yl)-5-[hydroxy(4-methylphenyl)methyl]phenol (9e)

To a solution of **17** (93 mg, 428 μmol, 1.0 eq) in anhydrous THF (2 mL) was added a 1 M solution of 4-tolylmagnesium bromide (1.00 mL, 195 mg, 1.00 mmol, 2.3 eq) in THF at rt, and the reaction solution was stirred for 1 h. To aid solubility, additional THF (2 mL) was added and the reaction solution was stirred at rt for 17 h. The reaction was quenched with a saturated aqueous solution of NH₄Cl (15 mL), and the aqueous phase was extracted with EtOAc (3 × 15 mL). The combined organic layers were washed with H₂O (45 mL), passed through an anhydrous frit and concentrated *in vacuo*. Purification by silica gel chromatography, eluting with acetone in petroleum ether (gradient elution 10 → 50%) afforded **9e** (75 mg, 56%) as a clear and colourless oil. Precipitation from Et₂O and hexane gave a colourless, amorphous solid: R_f (20% EtOAc/cyclohexane) 0.08; ν_{max} (thin film)/cm⁻¹: 3280 (br) (O–H), 1596 (s), 1421 (s); ¹H NMR (400 MHz, CD₃OD) δ 7.27 (2H, d, *J* = 7.9 Hz, C(3'')H & C(5'')H), 7.12 (2H, d, *J* = 7.9 Hz, C(2'')H & C(6'')H), 6.90–6.85 (1H, m, C(6'')H), 6.82–6.77 (1H, m, C(4'')H), 6.65–6.60 (1H, m, C(2'')H), 5.72 (1H, s, CHOH), 2.33 (3H, s, C(5')CH₃), 2.28 (3H, s, C(4'')CH₃), 2.19 (3H, s, C(3')CH₃); ¹³C NMR (126 MHz, CD₃OD) δ 166.4 (C(5')), 159.9 (C(3'')), 158.5 (C(1)), 148.1 (C(5)), 142.4 (C(1'')), 137.7 (C(4'')), 131.9 (C(3)), 129.5 (C(2'') & C(6'')), 127.3 (C(3'') & C(5'')), 119.3 (C(4)), 117.6 (C(4')), 115.2 (C(2)), 113.6 (C(6)), 76.1 (CHOH), 20.7 (C(4'')), 11.1 (C(5'')), 10.4 (C(3'')); HRMS *m/z* (ES⁺) Found: 310.1433. C₁₉H₂₀NO₄⁺ requires M⁺ 310.1438; LRMS (formic acid) RT = 0.92, [M + H]⁺ = 310; HPLC RT = 11.29 min, purity 98.5% (M1).

4.2.7. 3-(3,5-Dimethyl-1,2-oxazol-4-yl)-5-[(3,4-dichlorophenyl)(hydroxy)methyl]phenol (9f)

To a solution of **17** (110 mg, 506 μmol, 1.0 eq) in anhydrous THF (2 mL) was added a 0.5 M solution of 3,4-dichlorophenylmagnesium bromide (2.50 mL, 313 mg, 1.25 mmol, 2.5 eq) in THF at rt, and the reaction solution was stirred for 7 h, then was heated at 50 °C for 15 h. Additional 3,4-dichlorophenylmagnesium bromide (1.00 mL, 125 mg, 500 μmol, 1.0 eq) was added and the reaction solution was stirred at 50 °C for 7 h. The reaction was quenched with a saturated aqueous solution of NH₄Cl (15 mL), and the aqueous phase was extracted with EtOAc (3 × 15 mL). The combined organic layers were washed with H₂O (45 mL), passed through an anhydrous frit and concentrated *in vacuo*. The residue was resuspended in MeOH, filtered and the filtrate was concentrated *in vacuo*. Purification by silica gel chromatography, eluting with EtOAc in cyclohexane (gradient elution 5 → 55%) followed by mass-directed autopurification (0.1% formic acid, gradient elution MeCN/H₂O 30 → 85%) afforded **9f** (20 mg, 11%) as a colourless solid: R_f (50% EtOAc/cyclohexane) 0.49; ν_{max} (thin film)/cm⁻¹: 3198 (br) (O–H), 1637 (m), 1596 (s); ¹H NMR (400 MHz, CD₃OD) δ 7.58 (1H, d, *J* = 1.8 Hz, C(2'')H), 7.47 (1H, d, *J* = 8.3 Hz, C(5'')H), 7.31 (1H, dd, *J* = 8.3, 1.8 Hz, C(6'')H), 6.86–6.82 (1H, m, C(6'')H), 6.82–6.78 (1H, m, C(4'')H), 6.69–6.63 (1H, m, C(2'')H), 5.74 (1H, s, CHOH), 2.38 (3H, s, C(5')CH₃), 2.23 (3H, s, C(3')CH₃); ¹³C NMR (101 MHz, CD₃OD) δ 166.9 (C(5')), 160.0 (C(3'')), 159.2 (C(1)), 147.5 (C(3'')), 146.9 (C(4'')), 133.2 (C(3)), 132.7 (C(5)), 131.9 (C(1'')), 131.4 (C(5'')), 129.6 (C(2'')), 127.5 (C(6'')), 119.7 (C(4)), 117.9 (C(4')), 116.2 (C(2)), 113.9 (C(6)), 75.3 (CHOH), 11.5 (C(5')CH₃), 10.7 (C(3')CH₃); HRMS *m/z* (ES⁺) Found: 386.0322. C₁₈H₁₅Cl₂NNaO₃⁺ requires M⁺ 386.0321; LCMS (formic acid) RT = 1.05, [M + H]⁺ 364; HPLC RT = 13.52 min, purity 99.2% (M1).

4.2.8. 3-(3,5-Dimethyl-1,2-oxazol-4-yl)-5-[(4-fluorophenyl)(hydroxyl)methyl]phenol (9g)

Magnesium turnings (63 mg, 2.49 mmol, 6.0 eq) and a crystal of iodine were added to anhydrous THF (5 mL) and the mixture was stirred. 1-Bromo-4-fluorobenzene (314 μL, 500 mg, 2.85 mmol, 6.6 eq) in anhydrous THF (5 mL) were added to the dropping

funnel. The solution was added dropwise at rt, and the funnel was rinsed with further anhydrous THF (0.5 mL). The reaction mixture was heated under reflux with stirring for 1 h. After this time, the Mg turnings had dissolved and the solution became cloudy. The solution was cooled to 0 °C and an ice-cooled solution of **17** (94 mg, 433 μmol, 1.0 eq) in anhydrous THF (10 mL) added *via* cannulation. The reaction solution was warmed to rt and stirred for 16 h, then the reaction was quenched with H₂O (20 mL) and neutralised with an aqueous 1 M solution of HCl. The THF was removed *in vacuo*, and the aqueous phase was extracted with EtOAc (3 × 20 mL). The combined organic layers were washed with brine (30 mL), dried over anhydrous MgSO₄, filtered, and concentrated *in vacuo*. Purification by silica gel chromatography, eluting with EtOAc in petroleum ether (gradient elution 25 → 40%) afforded a colourless oil, from which **9g** was precipitated by the addition of CHCl₃ to give a colourless solid (98 mg, 72%); R_f (50% EtOAc/petroleum ether) 0.24; ν_{max} (thin film)/cm⁻¹: 3285 (br) (O–H), 2985 (m), 2972 (m), 2939 (m), 2923 (m), 2866 (m), 2844 (m), 2826 (m), 1597 (w); ¹H NMR (400 MHz, CD₃OD) δ 7.34–7.25 (2H, m, C(2'')H & C(6'')H), 6.98–6.89 (2H, m, C(3'')H & C(5'')H), 6.74–6.70 (1H, m, C(6)H), 6.69–6.64 (1H, m, C(4)H), 6.52–6.50 (1H, m, C(2)H), 5.63 (1H, s, CHOH), 2.25 (3H, s, C(5')CH₃), 2.10 (3H, s, C(3')CH₃); ¹³C NMR (126 MHz, CDCl₃) δ 166.4 (C(5')), 163.1 (d, J = 243.8 Hz, C(4')), 159.6 (C(3')), 158.7 (C(1)), 147.8 (C(5)), 141.6 (d, J = 2.9 Hz, C(1'')), 132.1 (C(3)), 129.2 (d, J = 8.2 Hz, C(2'') & C(6'')), 119.2 (C(4)H), 117.6 (C(4')), 115.51 (d, J = 29.3 Hz, C(3'') & C(5'')), 115.45 (C(2)H), 113.6 (C(6)H), 75.5 (CHOH), 11.1 (C(5')CH₃), 10.4 (C(3')CH₃); ¹⁹F NMR (377 MHz, CD₃OD) δ -117.7; HRMS *m/z* (ES⁺) Found: 336.1011. C₁₈H₁₆FNNaO₃⁺ requires M⁺ 336.1006; LRMS *m/z* (ES⁻) 312 ([M–H]⁻, 100%); HPLC RT = 11.03 min, purity 95.7% (M1).

4.2.9. 3-[Cyclohexyl(hydroxyl)methyl]-5-(3,5-dimethyl-1,2-oxazol-4-yl)phenol (9h)

Cyclohexanone (0.39 mL, 0.51 g, 3.1 mmol, 6.8 eq) in dry THF (1.0 mL) was added dropwise to a flask containing magnesium turnings (69 mg, 2.8 mmol, 6.1 eq) and a crystal of iodine in anhydrous THF (1.0 mL) at rt. Following initiation, the reaction solution was stirred for 1 h, then **17** (0.10 g, 0.46 mmol, 1.0 eq) in dry THF (2.0 mL) was added dropwise. The reaction solution was stirred at rt for 2 h then the reaction was quenched with a saturated aqueous solution of NH₄Cl (15 mL), and the aqueous phase was extracted with EtOAc (3 × 50 mL). The combined organic layers were washed with brine (50 mL), dried over anhydrous MgSO₄, filtered, and concentrated *in vacuo*. Purification by silica gel chromatography, eluting with EtOAc in petroleum ether (gradient elution 0 → 80%) afforded **9h** (103 mg, 74%) as a colourless solid foam: R_f (50% EtOAc/petroleum ether) 0.51; mp 84–86 °C (CHCl₃); ν_{max} (thin film)/cm⁻¹ 3273 (br) (O–H), 2927 (m), 2852 (w), 2363 (br), 1632 (w), 1595 (s), 1422 (s), 730 (s); ¹H NMR (500 MHz, CD₃OD) δ 6.77–6.74 (1H, m, C(4)H), 6.71–6.68 (1H, m, C(6)H), 6.53–6.50 (1H, m, C(2)H), 4.26 (1H, d, J = 7.2 Hz, CHOH), 2.39 (3H, s, C(5')CH₃), 2.24 (3H, s, C(3')CH₃), 2.03–1.96 (1H, m, CH), 1.80–1.73 (1H, m, CH), 1.72–1.61 (2H, m, 2 × CH), 1.61–1.52 (1H, m, CH), 1.45–1.37 (1H, m, CH), 1.31–0.84 (5H, m, 5 × CH); ¹³C NMR (126 MHz, CD₃OD) δ 166.7 (C(5')), 160.0 (C(3')), 158.8 (C(1)), 147.7 (C(5)), 132.0 (C(3)), 119.9 (C(4)), 118.1 (C(4')), 115.6 (C(2)), 114.2 (C(6)), 79.8 (CHOH), 46.4 (CHCHOH), 30.6 (CH₂), 30.2 (CH₂), 27.6 (CH₂), 27.3 (CH₂), 27.2 (CH₂), 11.5 (C(5')CH₃), 10.8 (C(3')CH₃); LRMS *m/z* (ES⁻) 300 ([M–H]⁻, 100%); HRMS *m/z* (ES⁺) found 302.17507 (100%), 303.17851 (30%); C₁₈H₂₃NO₃ requires [M + H]⁺ 302.17507; HPLC RT = 9.11 min, purity 99.3% (M2).

4.2.10. 3-[Cyclopropyl(hydroxyl)methyl]-5-(3,5-dimethyl-1,2-oxazol-4-yl)phenol (9i)

To a flask containing magnesium turnings (55 mg, 2.26 mmol, 6.1 eq) and a crystal of iodine was added dropwise bromocyclo-

propane (200 μL, 302 mg, 2.50 mmol, 6.8 eq) in anhydrous THF (2 mL). Following initiation, the reaction solution was stirred for 30 min, then **17** (80 mg, 368 μmol, 1.0 eq) and distilled THF (2 mL) were added. The reaction solution was stirred at rt for 18 h then the reaction was quenched with a saturated aqueous solution of NH₄Cl (15 mL), and the aqueous phase was extracted with EtOAc (3 × 15 mL). The combined organic layers were washed with H₂O (45 mL) and brine (45 mL), dried over anhydrous MgSO₄, filtered, and concentrated *in vacuo*. Purification by silica gel chromatography, eluting with EtOAc in petroleum ether (gradient elution 20 → 80%) afforded **9i** (81 mg, 85%) as a clear and colourless oil: R_f (50% EtOAc/petroleum ether) 0.24; ν_{max} (thin film)/cm⁻¹: 3240 (br) (O–H), 3001 (w), 2361 (w), 2343 (w), 1638 (w), 1597 (m); ¹H NMR (400 MHz, CD₃OD) δ 6.80–6.76 (1H, m, C(6)H), 6.74–6.70 (1H, m, C(4)H), 6.53 (1H, dd, J = 1.8, 1.8 Hz, C(2)H), 3.82 (1H, d, J = 8.3 Hz, CHOH), 2.30 (3H, s, C(5')CH₃), 2.15 (3H, s, C(3')CH₃), 1.09–0.98 (1H, m, CHCHOH), 0.55–0.46 (1H, m, CH), 0.45–0.31 (2H, m, 2 × CH), 0.29–0.22 (1H, m, CH); ¹³C NMR (101 MHz, CD₃OD) δ 166.8 (C(5')), 160.0 (C(3')), 158.9 (C(1)), 148.3 (C(5)), 132.2 (C(3)), 119.3 (C(4)), 118.1 (C(4')), 115.7 (C(2)), 113.6 (C(6)), 78.9 (CHOH), 19.8 (CHCHOH), 11.5 (C(5')CH₃), 10.8 (C(3')CH₃), 4.4 (CH₂), 3.1 (CH₂); HRMS *m/z* (ES⁺) Found: 282.1110. C₁₅H₁₇NaO₃⁺ requires M⁺ 282.1101; LRMS *m/z* (ES⁺) 260 ([M + H]⁺, 97%), 282 ([M + Na]⁺, 100%); HPLC RT = 9.98 min, purity 98.7% (M1).

4.2.11. 3-(3,5-Dimethyl-1,2-oxazol-4-yl)-5-[hydroxy(pyridine-3-yl)methyl]phenol (9j)

To a solution of 3-bromopyridine (351 mg, 2.22 mmol, 5.1 eq) in anhydrous THF (2 mL) was added a 1.3 M solution of isopropylmagnesium chloride lithium chloride complex (2.00 mL, 378 mg, 2.60 mmol, 6.0 eq) in THF dropwise at rt. The reaction mixture was stirred for 2 h, after which time a solution of **17** (94 mg, 433 μmol, 1.0 eq) in anhydrous THF (2 mL) was added dropwise, and the reaction solution stirred at rt for 4 h. The reaction was quenched with a saturated aqueous solution of NH₄Cl (15 mL), and the aqueous phase was extracted with EtOAc (3 × 15 mL). The combined organic layers were washed with H₂O (45 mL), brine (45 mL), dried over anhydrous MgSO₄, filtered, and concentrated *in vacuo*. Purification by silica gel chromatography, eluting with MeOH in CH₂Cl₂ (gradient elution 0 → 10%) afforded **9j** (94 mg, 73%) as a colourless solid: R_f (10% MeOH/CH₂Cl₂) 0.46; ν_{max} (thin film)/cm⁻¹: 2970 (br), 2949 (w), 2923 (br), 2866 (br), 2844 (w); ¹H NMR (400 MHz, DMSO-D₆) δ 9.57 (1H, s, C(1)OH), 8.62 (1H, d, J = 2.0 Hz, C(2'')H), 8.44 (1H, dd, J = 4.8, 2.0 Hz, C(6'')H), 7.76 (1H, ddd, J = 7.9, 2.0, 2.0 Hz, C(4'')H), 7.35 (1H, dd, J = 7.9, 4.8 Hz, C(5'')H), 6.87–6.76 (2H, m, C(4)H & C(6)H), 6.61 (1H, dd, J = 2.3, 1.6 Hz, C(2)H), 6.07 (1H, d, J = 4.0, CHOH), 5.75 (1H, d, J = 4.0, CHOH), 2.37 (3H, s, C(5')CH₃), 2.19 (3H, s, C(3')CH₃); ¹³C NMR (101 MHz, CD₃OD) δ 166.9 (C(5')), 159.9 (C(3')), 159.3 (C(1)), 148.8 (C(6'')), 148.6 (C(2'')), 147.4 (C(3'') or C(5)), 142.4 (C(5) or C(3'')), 136.4 (C(4'')), 132.8 (C(3)), 125.1 (C(5'')), 119.5 (C(4)), 117.8 (C(4')), 116.2 (C(2)), 113.9 (C(6)), 74.3 (CHOH), 11.5 (C(5')CH₃), 10.7 (C(3')CH₃); HRMS *m/z* (ES⁻) Found: 295.1092. C₁₇H₁₇N₂O₃⁻ requires M⁻ 295.1088; LRMS *m/z* (ES⁻) 295 ([M–H]⁻, 100%); HPLC RT = 8.29 min, purity 97.8% (M1).

4.2.12. 3-(3,5-Dimethyl-1,2-oxazol-4-yl)-5-[hydroxy(pyridine-4-yl)methyl]phenol (9k)

To a solution of 4-iodopyridine (242 mg, 1.18 mmol, 5.1 eq) in anhydrous THF (4 mL) was added a 2 M solution of isopropylmagnesium chloride (1.20 mL, 247 mg, 2.40 mmol, 10.3 eq) in THF dropwise at rt and the reaction solution was stirred for 1 h. To a solution of **17** (50 mg, 230 μmol, 1.0 eq) in anhydrous THF (4 mL) was added a portion of the above Grignard solution (2.60 mL, 590 μmol, 2.6 eq), and the solution was stirred at rt for 4 h, then was heated at 50 °C for 18 h. The reaction was quenched with a

saturated aqueous solution of NH_4Cl (15 mL), and the aqueous phase was extracted with EtOAc (3×15 mL). The combined organic layers were washed with H_2O (45 mL), passed through an anhydrous frit and concentrated *in vacuo*. Purification by silica gel chromatography, eluting with MeOH in CH_2Cl_2 (gradient elution 0 \rightarrow 20%) afforded **9k** (6 mg, 9%) as a yellow oil: R_f (10% EtOAc/cyclohexane) 0.40; ν_{max} (thin film)/ cm^{-1} : 3356 (br) (O–H), 2482 (br), 2244 (w), 2072 (m), 1598 (m); ^1H NMR (400 MHz, CD_3OD) δ 8.56–8.43 (2H, m, C(2'')H & C(6'')H), 7.53–7.48 (2H, m, C(3'')H & C(5'')H), 6.87–6.84 (1H, m, C(6)H), 6.84–6.81 (1H, m, C(4)H), 6.67 (1H, dd, $J = 2.2, 1.6$ Hz, C(2)H), 5.78 (1H, s, CHOH), 2.38 (3H, s, C(5') CH_3), 2.22 (3H, s, C(3') CH_3); ^{13}C NMR (101 MHz, CD_3OD) δ 166.9 (C(5')), 159.9 (C(3')), 159.3 (C(1)), 156.4 (C(5) or C(4')), 150.0 (C(2'')H & C(6'')H), 147.0 (C(4') or C(5)), 132.9 (C(3)), 123.0 (C(3'') & C(5'')), 119.8 (C(4)), 117.8 (C(4')), 116.4 (C(2)), 114.1 (C(6)), 75.2 (CHOH), 11.4 (C(5') CH_3), 10.7 (C(3') CH_3); HRMS m/z (ES^+) Found: 297.1238. $\text{C}_{17}\text{H}_{17}\text{N}_2\text{O}_3$ requires M^+ 297.11234; LRMS m/z (ES^+) 297 ([$\text{M} + \text{H}$] $^+$, 100%); HPLC RT = 8.27 min, purity 95.4% (M1).

4.2.13. 3-(3,5-Dimethyl-1,2-oxazol-4-yl)-5-[(3-fluorophenyl)(hydroxyl)methyl]phenol (9l)

To a solution of 1-fluoro-3-iodobenzene (270 μL , 511 mg, 2.30 mmol, 5.3 eq) in anhydrous THF (8 mL) was added a 1.3 M solution of isopropylmagnesium chloride lithium chloride (2.00 mL, 378 mg, 2.60 mmol, 5.8 eq) in THF dropwise at -10°C . The reaction solution was warmed to rt and stirred for 5 h. To a solution of **17** (94 mg, 433 μmol , 1.0 eq) in anhydrous THF (8 mL) was added dropwise a portion of the above Grignard solution (4.00 mL, 909 μmol , 2.1 eq). The reaction was stirred at rt for 3 h, then was heated at 50°C for 18 h. Additional Grignard solution (1.00 mL, 227 μmol , 0.5 eq) was added and the reaction solution was heated at 50°C for 2 h, before addition of the remaining Grignard solution (5.00 mL, 1.15 mmol, 2.7 eq). The reaction solution was stirred at 50°C for 1 h, then the reaction was quenched with a saturated aqueous solution of NH_4Cl (15 mL), and the aqueous phase was extracted with EtOAc (3×15 mL). The combined organic layers were washed with H_2O (45 mL), passed through an anhydrous frit and concentrated *in vacuo*. Purification by silica gel chromatography, eluting with EtOAc in cyclohexane (gradient elution 5 \rightarrow 100%) followed by mass-directed autopurification (0.1% formic acid, gradient elution MeCN / H_2O 15 \rightarrow 55%) afforded **9l** (15 mg, 11%) as a clear and colourless oil that solidified under vacuum to give a colourless, amorphous solid: R_f (50% EtOAc/petroleum ether) 0.49; ν_{max} (thin film)/ cm^{-1} : 3291 (br) (O–H), 2470 (br), 1593 (s); ^1H NMR (400 MHz, CD_3OD) δ 7.37–7.29 (1H, m, C(5'')H), 7.24–7.19 (1H, m, C(6)H), 7.19–7.13 (1H, m, C(2'')H or C(4'')H), 7.01–7.93 (1H, m, C(4'')H or C(2'')H), 6.88–8.83 (1H, m, C(6)H), 6.82–6.78 (1H, m, C(4)H), 6.67–6.62 (1H, m, C(2)H), 5.76 (1H, s, CHOH), 2.38 (3H, s, C(5') CH_3), 2.22 (3H, s, C(3') CH_3); ^{13}C NMR (101 MHz, CD_3OD) δ 168.8 (C(5')), 164.3 (d, $J = 245$ Hz, C(3'')), 159.9 (C(3')), 159.1 (C(1)), 148.9 (d, $J = 7$ Hz, C(1'')), 147.9 (C(5)), 132.5 (C(3)), 131.0 (d, $J = 8$ Hz, C(5'')), 123.4 (d, $J = 3$ Hz, C(6'')), 119.7 (C(4)), 117.9 (C(4')), 115.9 (C(2)), 114.8 (d, $J = 21$ Hz, C(2'') or C(4'')), 114.1 (d, $J = 22$ Hz, C(4'') or C(2'')), 114.0 (C(6)), 75.9 (CHOH), 11.4 (C(5') CH_3), 10.7 (C(3') CH_3); ^{19}F NMR (377 MHz, CD_3OD) δ -115.4 ; HRMS m/z (ES^-) Found: 312.1043. $\text{C}_{18}\text{H}_{15}\text{FNO}_3$ requires M^- 312.1041; LRMS m/z (ES^-) 312 ([$\text{M} - \text{H}$] $^-$, 100%); HPLC RT = 11.08 min, purity 95.4% (M1).

4.2.14. 3-[[3-(3,5-Dimethyl-1,2-oxazol-4-yl)-5-hydroxyphenyl](hydroxyl)methyl]benzotrile (9m)

To a solution of 4-iodobenzotrile (484 mg, 2.11 mmol, 4.4 eq) in anhydrous THF (2 mL) was added a 1.3 M solution of isopropylmagnesium chloride lithium chloride complex (2.00 mL, 378 mg, 2.60 mmol, 5.4 eq) in THF dropwise at -10°C . The reaction solution was stirred for 4 h. To a solution of **17** (105 mg, 483 μmol , 1.0 eq) in

anhydrous THF (8 mL) at -10°C was added dropwise the Grignard solution. The solution was stirred for 3 h, then was warmed to rt and quenched with a saturated aqueous solution of NH_4Cl (15 mL), and the aqueous phase was extracted with EtOAc (3×15 mL). The combined organic layers were washed with H_2O (45 mL) and brine (45 mL), dried over anhydrous MgSO_4 , filtered, and concentrated *in vacuo*. Purification by silica gel chromatography, eluting with EtOAc in petroleum ether (gradient elution 10 \rightarrow 60%) afforded **9m** (34 mg, 23%) as a clear and colourless oil: R_f (50% EtOAc/petroleum ether) 0.32; ν_{max} (thin film)/ cm^{-1} : 3319 (br) (O–H), 2972 (w), 2230 (w) (C \equiv N), 1632 (w), 1595 (m); ^1H NMR (400 MHz, CD_3OD) δ 7.71–7.66 (2H, m, C(3'')H & C(5'')H), 7.62–7.57 (2H, m, C(2'')H & C(6'')H), 6.83–6.80 (1H, m, C(6)H), 6.79–6.77 (1H, m, C(4)H), 6.79–6.77 (1H, m, C(2)H), 5.79 (1H, s, CHOH), 2.36 (3H, s, C(5') CH_3), 2.20 (3H, s, C(3') CH_3); ^{13}C NMR (126 MHz, CD_3OD) δ 165.5 (C(5')), 158.5 (C(3')), 157.8 (C(1)), 150.3 (C(5)), 146.0 (C \equiv N), 131.9 (C(3'') and C(5'')), 131.3 (C(3)), 127.0 (C(2'') and C(6'')), 118.4 (C(4'')), 118.3 (C(4)), 116.4 (C(4')), 114.7 (C(2)), 112.6 (C(6)), 110.5 (C(1'')), 74.5 (CHOH), 10.0 (C(5') CH_3), 9.3 (C(3') CH_3); HRMS m/z (ES^+) Found: 343.1061. $\text{C}_{19}\text{H}_{16}\text{N}_2\text{O}_3$ requires M^+ 343.1053; LRMS m/z (ES^-) 319 ([$\text{M} - \text{H}$] $^-$, 52%), 639 ([$2\text{M} - \text{H}$] $^-$, 100%); HPLC RT = 10.83 min, purity 95.7% (M1).

4.2.15. 3-[(5-Chloropyridin-2-yl)(hydroxyl)methyl]-5-(3,5-dimethyl-1,2-oxazol-4-yl)phenol (9n)

To a solution of 5-chloro-2-iodopyridine (532 mg, 2.22 mmol, 5.1 eq) in anhydrous THF (2 mL) was added a 1.3 M solution of isopropylmagnesium chloride lithium chloride complex (2.00 mL, 378 mg, 2.60 mmol, 6.0 eq) in THF dropwise at rt. The reaction solution was stirred for 2 h. To a solution of **17** (94 mg, 433 μmol , 1.0 eq) in anhydrous THF (2 mL) was added dropwise a portion of the above Grignard solution (2.00 mL, 1.11 mmol, 2.6 eq). The reaction was stirred at rt for 23 h, then was heated at 50°C for 21 h, before the remaining Grignard solution (2.00 mL, 1.11 mmol, 2.6 eq) was added. The reaction solution was stirred for a further 5 h at 50°C , then the reaction was quenched with a saturated aqueous solution of NH_4Cl (15 mL), and the aqueous phase was extracted with EtOAc (3×15 mL). The combined organic layers were washed with H_2O (45 mL) and brine (45 mL), dried over anhydrous MgSO_4 , filtered, and concentrated *in vacuo*. Purification by silica gel chromatography, eluting with acetone in petroleum ether (gradient elution 20 \rightarrow 80%) afforded **9n** (22 mg, 15%) as a clear and colourless oil. Precipitation from CHCl_3 and hexane afforded **9n** as a colourless amorphous solid: R_f (50% EtOAc/cyclohexane) 0.35; ν_{max} (thin film)/ cm^{-1} : 3457 (br), 3016 (br) (O–H), 2970 (w), 2837 (w), 1631 (m), 1369 (s); ^1H NMR (400 MHz, CD_3OD) δ 8.45 (1H, d, $J = 2.4$ Hz, C(6'')H), 7.85 (1H, dd, $J = 8.5, 2.4$ Hz, C(4'')H), 7.61 (1H, d, $J = 8.5$ Hz, C(3'')H), 6.87–6.80 (2H, m, C(4)H and C(6)H), 6.61 (1H, dd, $J = 1.8, 1.8$ Hz, C(2)H), 5.76 (1H, s, CHOH), 2.36 (3H, s, C(5') CH_3), 2.20 (3H, s, C(3') CH_3); ^{13}C NMR (126 MHz, CD_3OD) δ 166.9 (C(5')), 163.1 (C(2'')), 159.9 (C(3')), 159.2 (C(1)), 148.1 (C(6'')), 146.6 (C(5)), 138.3 (C(4'')), 132.6 (C(3)), 131.9 (C(5'')), 123.1 (C(3'')), 119.6 (C(6)), 117.8 (C(4'')), 116.1 (C(2)), 114.0 (C(4)), 76.7 (CHOH), 11.4 (C(5') CH_3), 10.7 (C(3') CH_3); HRMS m/z (ES^+) Found: 353.0659. $\text{C}_{17}\text{H}_{15}\text{ClN}_2\text{O}_3$ requires M^+ 353.0663; LRMS m/z (ES^-) 329 ([$\text{M} - \text{H}$] $^-$, 100%); HPLC RT = 9.93 min, purity 97.2% (M1).

4.2.16. 3-(3,5-Dimethyl-1,2-oxazol-4-yl)-5-[(2-fluorophenyl)(hydroxyl)methyl]phenol (9o)

To a solution of 1-bromo-2-fluorobenzene (27.0 μL , 43 mg, 247 μmol , 1.2 eq) in anhydrous THF (2 mL) at -78°C was added a 2.3 M solution of $^n\text{BuLi}$ in THF (12.0 μL , 28 mg, 431 μmol , 2.1 eq). The reaction solution was stirred at -78°C for 40 min before a solution of **18** (75 mg, 201 μmol , 1.0 eq) in anhydrous THF (2 mL) was added. The solution was stirred at -78°C for 3 h, then was warmed to rt and quenched with H_2O (5 mL) and neutralised with an aqueous

ous 1 M solution of HCl. The THF was removed *in vacuo*, and the aqueous phase was extracted with EtOAc (3 × 10 mL). The combined organic layers were washed with H₂O (30 mL) and brine (30 mL), dried over anhydrous MgSO₄, filtered, and concentrated *in vacuo*. To a solution of the resulting residue in distilled THF (5 mL) at 0 °C was added a 1 M solution of TBAF (65.0 μL, 59 mg, 224 μmol, 1.1 eq) in THF. The solution was stirred at 0 °C for 2 h, then the volatile components were removed *in vacuo*. The resulting residue was partitioned between H₂O (10 mL) and EtOAc (10 mL). The phases were separated, the aqueous layer was extracted with EtOAc (2 × 10 mL) and the combined organic layers were washed with brine (30 mL), dried over anhydrous MgSO₄, filtered, and concentrated *in vacuo*. Purification by silica gel chromatography, eluting with EtOAc in petroleum ether (gradient elution 20 → 100%) afforded **9o** (11 mg, 17%) as a clear and colourless oil, which was precipitated from CHCl₃ with hexane to give a colourless, amorphous solid: R_f (50% EtOAc/petroleum ether) 0.45; ν_{max} (thin film)/cm⁻¹: 2970 (w), 2866 (br), 2844 (br), 1739 (s), 1435 (w), 1371 (w); ¹H NMR (500 MHz, CD₃OD) δ 7.56 (1H, ddd, J = 7.6, 7.6, 1.6 Hz, C(6''H)), 7.30–7.24 (1H, m, C(4''H)), 7.17 (1H, ddd, J = 7.6, 7.6, 1.0 Hz, C(5''H)), 7.04 (1H, ddd, J = 10.5, 8.1, 1.0 Hz, C(3''H)), 6.84–6.82 (1H, m, C(6)H), 6.78–6.76 (1H, m, C(4)H), 6.62–6.60 (1H, m, C(2)H), 6.03 (1H, s, CHOH), 2.35 (3H, s, C(5')CH₃), 2.19 (3H, s, C(3')CH₃); ¹³C NMR (126 MHz, CD₃OD) δ 166.8 (C(5')), 161.2 (d, J = 244 Hz, C(2'')), 159.9 (C(3')), 159.0 (C(1)), 147.3 (C(5)), 132.9 (d, J = 13 Hz, C(1'')), 132.4 (C(3)), 130.1 (d, J = 8 Hz, C(5'')), 128.8 (d, J = 4 Hz, C(3'')), 125.4 (d, J = 3 Hz, C(4'')), 119.5 (C(4)), 117.9 (C(4')), 116.1 (d, J = 22 Hz, C(6')), 115.8 (C(2)), 113.9 (C(6)), 69.9 (d, J = 3 Hz, CHOH), 11.4 (C(5')CH₃), 10.7 (C(3')CH₃); ¹⁹F NMR (377 MHz, CD₃OD) δ -120.6; HRMS *m/z* (ES⁺) Found: 336.1013. C₁₈H₁₆FNNaO₃ requires M⁺ 336.1006; LRMS *m/z* (ES⁺) 314 ([M + H]⁺, 100%); HPLC RT = 11.00 min, purity 95.2% (M1).

4.2.17. 3-(3,5-Dimethyl-1,2-oxazol-4-yl)-5-[hydroxy(pyridine-2-yl)methyl]phenol (9p)

To a solution of 2-bromopyridine (38.0 μL, 64 mg, 402 μmol, 1.5 eq) in Et₂O (3 mL) at -78 °C was added a 2.3 M solution of ^tBuLi in hexanes (180 μL, 420 mg, 414 μmol, 1.5 eq). The reaction solution was stirred at -78 °C for 40 min, then was warmed to rt and stirred for a further 40 min before cooling to -78 °C. To this was added a solution of **18** (100 mg, 268 μmol, 1.0 eq) in Et₂O (5 mL). The solution was allowed to warm to rt, over 16 h then the reaction was quenched with H₂O (5 mL) and neutralised with an aqueous 20% (w/v) solution of NH₄Cl. The aqueous phase was extracted with EtOAc (4 × 10 mL). The combined organic layers were washed with brine (40 mL), dried over anhydrous Na₂SO₄, filtered, and concentrated *in vacuo*. Purification by silica gel chromatography, eluting with EtOAc in 30–40 °C petroleum ether (gradient elution 4 → 50%) afforded the TIPS-protected intermediate (65 mg, 54%) as a yellow oil. To a solution of this intermediate (50 mg, 110 μmol, 1.0 eq) in distilled THF (2 mL) at 0 °C was added a 1 M solution of TBAF (121 μL, 110 mg, 121 μmol, 1.1 eq). The reaction was stirred at 0 °C for 30 min, then the volatile components were removed *in vacuo*. Purification by silica gel chromatography, eluting with acetone in 30–40 °C petroleum ether (gradient elution 20 → 60%) afforded **9p** (29 mg, 89%) as a colourless solid: R_f (40% EtOAc/petroleum ether) 0.26; mp 221–223 °C (acetone); ν_{max} (thin film)/cm⁻¹: 3389 (br), 2925 (w), 1593 (s); ¹H NMR (400 MHz, DMSO-D₆) δ 9.53 (1H, s, C(1)OH), 8.48–8.43 (1H, m, C(6''H)), 7.78 (1H, ddd, J = 9.5, 7.6, 1.8 Hz, C(4''H)), 7.59–7.54 (1H, m, C(3''H)), 7.24 (1H, ddd, J = 7.6, 4.9, 1.1 Hz, C(5''H)), 6.84–6.79 (2H, m, C(4)H & C(6)H), 6.59–6.56 (1H, m, C(2)H), 6.08 (1H, d, J = 4.1 Hz, CHOH), 5.66 (1H, d, J = 4.1, CHOH), 2.35 (3H, s, C(5')CH₃), 2.17 (3H, s, C(3')CH₃); ¹³C NMR (126 MHz, DMSO-D₆) δ 164.9 (C(5')), 163.9 (C(3')), 157.9 (C(1)), 157.4 (C(2'')), 148.3 (C(6'')), 146.4 (C(5)), 136.8 (C(4'')), 130.5 (C(3)), 122.2 (C(5'')), 120.0 (C(3'')), 117.7 (C(4)),

115.9 (C(4')), 114.1 (C(2)), 112.4 (C(6)), 75.4 (CHOH), 11.3 (C(5')CH₃), 10.5 (C(3')CH₃); HRMS *m/z* (ES⁺) Found: 319.1048. C₁₇H₁₇N₂-NaO₃ requires M⁺ 319.1053; LRMS *m/z* (ES⁺) 297 ([M + H]⁺, 100%), 319 ([M + Na]⁺, 20%); HPLC RT = 8.42 min, purity 98.9% (M1).

4.2.18. 3-(3,5-Dimethyl-1,2-oxazol-4-yl)-5-[(4-methylpiperazin-1-yl)methyl]phenol (10a)

To a solution of **17** (106 mg, 488 μmol, 1.0 eq) and 1-methylpiperazine (70.0 μL, 63 mg, 631 μmol, 1.3 eq) in EtOH (5 mL) was added AcOH dropwise until the solution was pH 4. The reaction solution was stirred at rt for 20 min before addition of NaBH₃CN (20 mg, 318 μmol, 0.7 eq). The solution was stirred for a further 17 h and the volatile components were removed *in vacuo*. Purification by silica gel chromatography, eluting with MeOH in CH₂Cl₂ (gradient elution 0 → 20%) yielded **10a** (101 mg, 69%) as an oil that crystallised under vacuum. A small sample of **10a** was purified by semi-preparative HPLC for biological testing. The degree of TFA salt formation was quantified using 1,4-difluorobenzene (DFB) as an internal standard in ¹⁹F NMR and gave a TFA content of 19.2% (w/w). The difference in relaxation times of ¹⁹F nuclei of TFA and DFB was addressed by an external calibration using samples containing known amounts of TFA and DFB. R_f (20% MeOH/CH₂Cl₂) 0.43; mp free amine 144–146 °C (MeOH), TFA salt (from MeCN) > 250 °C; ν_{max} (thin film)/cm⁻¹: 2965 (w), 2813 (w), 1589 (m); ¹H NMR (400 MHz, CD₃OD) δ 6.91–6.84 (2H, m, C(4)H & C(6)H), 6.79–6.74 (1H, m, C(2)H), 3.99 (2H, s, CH₂Ar), 3.53–3.36 (4H, m, 4 × NCH₂), 3.28–3.04 (4H, m, 4 × NCH₂), 2.92 (3H, s, NCH₃), 2.41 (3H, s, C(5')CH₃), 2.25 (3H, s, C(3')CH₃); ¹³C NMR (126 MHz, CD₃OD) δ 167.0 (C(5')H), 159.9 (C(3')H), 159.5 (C(1)), 137.6 (C(3)), 132.5 (C(5)), 122.5 (C(4)), 117.6 (C(2)), 115.8 (C(6)), 114.1 (C(4')), 62.0 (CH₂Ar), 53.8 (2 × NCH₂), 50.5 (2 × NCH₂), 43.5 (CH₃), 11.4 (C(5')CH₃), 10.7 (C(3')CH₃); ¹⁹F NMR (377 MHz, CD₃OD) δ -77.3; HRMS *m/z* (ES⁺) Found: 302.1858. C₁₇H₂₄N₃O₂ requires M⁺ 302.1863; LRMS *m/z* (ES⁺) 302 ([M + H]⁺, 100%); HPLC RT = 8.14 min, purity 99.7% (M1).

4.2.19. 3-(3,5-Dimethyl-1,2-oxazol-4-yl)-5-(morpholin-4-ylmethyl)phenol (10b)

To a solution of **17** (100 mg, 460 μmol, 1.0 eq) and morpholine (50.0 μL, 50 mg, 572 μmol, 1.2 eq) in EtOH (5 mL) was added AcOH dropwise until the solution was pH 4. The reaction solution was stirred at rt for 40 min before addition of NaBH₃CN (23 mg, 366 μmol, 0.8 eq). The solution was stirred for a further 23 h and the volatile components were removed *in vacuo*. Purification by silica gel chromatography, eluting with EtOAc in petroleum ether (gradient elution 40 → 100%) yielded **10b** (27 mg, 20%) as a yellow oil. A small sample of **10b** was purified by semi-preparative HPLC for biological testing. The degree of TFA salt formation was quantified using 1,4-difluorobenzene (DFB) as an internal standard in ¹⁹F NMR and gave a TFA content of 23.9% (w/w). The difference in relaxation times of ¹⁹F nuclei of TFA and DFB was addressed by an external calibration using samples containing known amounts of TFA and DFB. R_f (80% EtOAc/petroleum ether) 0.10; ν_{max} (thin film)/cm⁻¹: 2982 (m), 2886 (w), 2359 (m), 2344 (m), 1673 (m); mp TFA salt (MeCN) > 250 °C; ¹H NMR (400 MHz, CD₃OD) δ 6.97 (1H, dd, J = 1.9, 1.9 Hz, C(4)H), 6.94 (1H, dd, J = 1.4, 1.4 Hz, C(6)H), 6.88 (1H, dd, J = 1.9, 1.4 Hz, C(2)H), 4.34 (2H, s, CH₂Ar), 4.19–3.94 (2H, m, 2 × CH_AH_B), 3.87–3.63 (2H, m, 2 × CH_AH_B), 3.50–3.07 (4H, m, 2 × CH₂), 2.42 (3H, s, C(5')CH₃), 2.27 (3H, s, C(3')CH₃); ¹³C NMR (126 MHz, CD₃OD) δ 167.2 (C(5')), 160.0 (C(3')), 159.8 (C(1)), 133.9 (C(3)), 131.7 (C(5)), 123.8 (C(4)), 118.7 (C(2)H), 118.4 (C(6)), 117.1 (C(4')), 64.9 (2 × CH₂O), 61.7 (CH₂Ar), 52.9 (2 × CH₂N), 11.5 (C(5')CH₃), 10.7 (C(3')CH₃); ¹⁹F NMR (377 MHz, CD₃OD) δ -77.1; HRMS *m/z* (ES⁺) Found: 289.1547. C₁₆H₂₁N₂O₃ requires M⁺ 289.1547; LRMS *m/z* (ES⁺) 289 ([M + H]⁺, 100%); HPLC RT = 8.58 min, purity 99.5% (M1).

4.2.20. 3-[(Benzylamino)methyl]-5-(3,5-dimethyl-1,2-oxazol-4-yl)phenol (10c)

To a solution of benzylamine (100 μL , 98 mg, 916 μmol , 1.9 eq) and AcOH (100 μL , 104 mg, 1.75 mmol, 3.6 eq) in EtOH (5 mL) was added **17** (105 mg, 483 μmol , 1.0 eq). The reaction solution was stirred at rt for 30 min, then NaBH_3CN (39 mg, 621 μmol , 1.3 eq) was added. The solution was stirred for a further 19 h, then the volatile components were removed *in vacuo*. Purification by silica gel chromatography, eluting with EtOH in EtOAc (gradient elution 0 \rightarrow 50%), followed by ISOLUTE[®] SCX-2 amine catch and release column yielded **10c** (103 mg, 69%) as a clear and colourless oil. A small sample of **10c** was purified by semi-preparative HPLC for biological testing. The degree of TFA salt formation was quantified using 1,4-difluorobenzene (DFB) as an internal standard in ¹⁹F NMR and gave a TFA content of 18.6% (w/w). The difference in relaxation times of ¹⁹F nuclei of TFA and DFB was addressed by an external calibration using samples containing known amounts of TFA and DFB. R_f free amine (70% EtOAc/petroleum ether) 0.18; ν_{max} (thin film)/ cm^{-1} : 2982 (w), 2361 (m), 2344 (m), 1670 (m); mp TFA salt > 250 °C (MeCN); ¹H NMR (500 MHz, CD₃OD) δ 7.52–7.44 (5H, m, C₆H₅), 6.95–6.92 (1H, m, C(6)H), 6.91–6.88 (1H, m, C(4)H), 6.84–6.81 (1H, m, C(2)H), 4.26 (2H, s, CH₂Ph), 4.22 (2H, s, CH₂Ar), 2.41 (3H, s, C(5')CH₃), 2.25 (3H, s, C(3')CH₃); ¹³C NMR (126 MHz, CDCl₃) δ 167.2 (C(5')), 159.8 (C(3')) & (C(1)), 134.5 (C(5)), 133.8 (C(3)), 132.4 (C(1')), 131.1 (C(2'') & C(6'') or C(3'') & C(5'')), 130.8 (C(4'')), 130.3 (C(3'') & C(5'') or C(2'') & C(6'')), 122.4 (C(4)), 118.1 (C(2)), 117.4 (C(4')), 117.2 (C(6)), 52.2 (CH₂Ph), 51.8 (CH₂Ar), 11.5 (C(5')CH₃), 10.7 (C(3')CH₃); ¹⁹F NMR (377 MHz, CD₃OD) δ -77.1; HRMS m/z (ES⁺) Found: 309.1592. C₁₉H₂₁O₂N₂ requires M⁺ 309.1598; LRMS m/z (ES⁺) 309 ([M + H]⁺, 100%); HPLC RT = 9.67 min, purity 97.7% (M1).

4.2.21. 3-(3,5-Dimethyl-1,2-oxazol-4-yl)-5-(4,4-difluoropiperidin-1-ylmethyl)phenol (10d)

To a solution of 4,4-difluoropiperidine hydrochloride (156 mg, 987 μmol , 2.1 eq) in EtOH (5 mL) was added **17** (100 mg, 460 μmol , 1.0 eq). The reaction solution was stirred at rt for 30 min, then NaBH_3CN (49 mg, 780 μmol , 1.6 eq) was added. The solution was stirred for a further 19 h, then the volatile components were removed *in vacuo*. Purification by silica gel chromatography, eluting with EtOAc in petroleum ether (gradient elution 15 \rightarrow 100%), followed by ISOLUTE[®] SCX-2 amine catch and release column yielded **10d** (49 mg, 33%) as a clear and colourless oil. A small sample of the **10d** was purified by semi-preparative HPLC before biological evaluation. The degree of protonation was quantified by ¹⁹F NMR and gave a TFA content of 31.5% (w/w). R_f free amine (100% EtOAc) 0.69; ν_{max} (thin film)/ cm^{-1} : 2982 (m), 2886 (w), 2359 (m), 2344 (m), 2160 (w); mp TFA salt > 250 °C (MeCN); ¹H NMR (400 MHz, CD₃OD) δ 6.99–6.96 (1H, m, C(6)H), 6.94 (1H, dd, $J = 1.4, 1.4$ Hz, C(4)H), 6.90–6.87 (1H, m, C(2)H), 4.37 (2H, s, CH₂Ar), 3.71–3.22 (4H, m, 2 \times NCH₂), 2.48–2.23 (4H, m, 2 \times CF₂CH₂), 2.42 (3H, s, C(5')CH₃), 2.27 (3H, s, C(3')CH₃); ¹³C NMR (126 MHz, CDCl₃) δ 167.2 (C(5')), 160.0 (C(3')), 159.8 (C(1)), 134.0 (C(3)), 132.5 (C(5)), 123.5 (C(4)), 120.2 (t, $J = 242$ Hz, CF₂), 118.7 (C(6)), 118.2 (C(2)), 117.1 (C(4')), 60.7 (CH₂Ar), 50.4 (t, $J = 6$ Hz, 2 \times NCH₂), 32.1 (t, $J = 26$ Hz, 2 \times CF₂CH₂), 11.5 (C(5')CH₃), 10.7 (C(3')CH₃); ¹⁹F NMR (377 MHz, CD₃OD) δ -77.0 (CF₃CO₂), -98.7 (1F, d, $J = 195$ Hz, CF_AF_B), -104.9 (1F, d, $J = 195$ Hz, CF_AF_B); HRMS m/z (ES⁺) Found: 323.1560. C₁₇H₂₁O₂N₂F₂ requires M⁺ 323.1566; LRMS m/z (ES⁺) 323 ([M + H]⁺, 100%); HPLC RT = 9.29 min, purity 99.6% (M1).

4.2.22. 3-(3,5-Dimethyl-1,2-oxazol-4-yl)-5-(piperidin-1-ylmethyl)phenol (10e)

To a solution of piperidine (50.0 μL , 43 mg, 506 μmol , 1.5 eq) and AcOH (50.0 μL , 52 mg, 873 μmol , 2.7 eq) in EtOH (5 mL) was

added **18** (123 mg, 329 μmol , 1.0 eq). The reaction solution was stirred at rt for 1 h, then NaBH_3CN (11 mg, 175 μmol , 0.5 eq) was added. The solution was stirred for a further 22 h, then the volatile components were removed *in vacuo*. Purification by silica gel chromatography, eluting with EtOAc in petroleum ether (gradient elution 0 \rightarrow 50%), followed by ISOLUTE[®] SCX-2 amine catch and release column yielded an oil that contained a mixture of **10e** (1 mg, 3.49 μmol) and the TIPS-protected intermediate (14 mg, 31.6 μmol). To a solution of the oil resuspended in distilled THF (1 mL) was added a 1 M solution of TBAF (35.0 μL , 32 mg, 35.0 μmol , 1.1 eq) in THF dropwise at 0 °C. The reaction was warmed to rt and stirred for 2 h, then the reaction was quenched with H₂O (5 mL). The aqueous phase was extracted with EtOAc (3 \times 5 mL), and the combined organic layers were washed with brine (15 mL), dried over anhydrous MgSO₄, filtered, and concentrated *in vacuo*. Purification by silica gel chromatography, eluting with EtOH in EtOAc (gradient elution 0 \rightarrow 50%) yielded **10e** (11 mg, 8%) as a clear and colourless oil: R_f (20% MeOH/CH₂Cl₂) 0.56; ν_{max} (thin film)/ cm^{-1} : 2982 (w), 2938 (w), 2361 (m), 2334 (m); ¹H NMR (500 MHz, CD₃OD) δ 6.79 (1H, dd, $J = 1.8, 1.8$ Hz, C(4)H), 6.77–6.64 (1H, m, C(6)H), 6.65 (1H, dd, $J = 1.8, 1.8$ Hz, C(2)H), 3.48 (2H, s, CH₂Ar), 2.52–2.40 (4H, m, 2 \times CH₂N), 2.40 (3H, s, C(5')CH₃), 2.25 (3H, s, C(3')CH₃), 1.61 (4H, tt, $J = 5.7, 5.7$ Hz, 2 \times CH₂CH₂N), 1.53–1.32 (2H, m, CH₂-CH₂CH₂N); ¹³C NMR (126 MHz, CD₃OD) δ 166.8 (C(5')), 160.0 (C(3')), 159.1 (C(1)), 140.5 (C(5)), 132.4 (C(3)), 122.6 (C(4)), 117.9 (C(4')), 117.2 (C(6)), 116.0 (C(2)), 64.5 (CH₂Ar), 55.4 (2 \times CH₂N), 26.5 (2 \times CH₂CH₂N), 25.1 (CH₂CH₂CH₂N), 11.5 (C(5')CH₃), 10.7 (C(3')CH₃); HRMS m/z (ES⁺) Found: 287.1759. C₁₇H₂₃N₂O₂ requires M⁺ 287.1754; LRMS m/z (ES⁺) 287 ([M + H]⁺, 100%); HPLC RT = 9.24 min, purity 99.2% (M1).

4.2.23. 3-(3,5-Dimethyl-1,2-oxazol-4-yl)-5-(pyrrolidin-1-ylmethyl)phenol (10f)

To a solution of pyrrolidine (50.0 μL , 43 mg, 493 μmol , 1.3 eq) and AcOH (50.0 μL , 52 mg, 873 μmol , 2.4 eq) in EtOH (5 mL) was added **18** (138 mg, 369 μmol , 1.0 eq). The reaction solution was stirred at rt for 1 h, then NaBH_3CN (13 mg, 207 μmol , 0.6 eq) was added. The solution was stirred for a further 22 h, then the volatile components were removed *in vacuo*. Purification by silica gel chromatography, eluting with EtOAc in petroleum ether (gradient elution 0 \rightarrow 50%), followed by ISOLUTE[®] SCX-2 amine catch and release column yielded an oil that contained a mixture of **10f** (10 mg, 3.67 μmol) and the TIPS-protected intermediate (54 mg, 126 μmol). To a solution of the oil resuspended in distilled THF (2 mL) was added a 1 M solution of TBAF (200 μL , 181 mg, 200 μmol , 1.6 eq) in THF dropwise at 0 °C. The reaction was warmed to rt and stirred for 1 h, then the reaction was quenched with H₂O (5 mL). The aqueous phase was extracted with EtOAc (3 \times 5 mL), and the combined organic layers were washed with brine (15 mL), dried over anhydrous MgSO₄, filtered, and concentrated *in vacuo*. Purification by silica gel chromatography, eluting with EtOH in EtOAc (gradient elution 0 \rightarrow 40%) yielded **10f** (33 mg, 33%) as a clear and colourless oil: R_f (20% MeOH/CH₂Cl₂) 0.44; ν_{max} (thin film)/ cm^{-1} : 2961 (m), 2930 (m), 1632 (w), 1593 (s); ¹H NMR (500 MHz, CD₃OD) δ 6.81 (1H, dd, $J = 1.7, 1.7$ Hz, C(4)H), 6.79–6.77 (1H, m, C(6)H), 6.66 (1H, dd, $J = 2.2, 1.7$ Hz, C(2)H), 3.66 (2H, s, CH₂-Ar), 2.67–2.60 (4H, m, 2 \times CH₂N), 2.39 (3H, s, C(5')CH₃), 2.24 (3H, s, C(3')CH₃), 1.87–1.80 (4H, m, 2 \times CH₂CH₂N); ¹³C NMR (126 MHz, CD₃OD) δ 166.8 (C(5')), 159.9 (C(3')), 159.2 (C(1)), 141.0 (C(5)), 132.6 (C(3)), 122.3 (C(4)), 117.8 (C(4')), 116.8 (C(6)), 116.2 (C(2)), 61.1 (CH₂Ar), 54.9 (2 \times CH₂N), 24.1 (2 \times CH₂CH₂N), 11.5 (C(5')CH₃), 10.7 (C(3')CH₃); HRMS m/z (ES⁺) Found: 273.1597. C₁₆H₂₁N₂O₂ requires M⁺ 273.1598; LRMS m/z (ES⁺) 273 ([M + H]⁺, 100%); HPLC RT = 8.98 min, purity 95.9% (M1).

4.2.24. 3-Benzyl-5-(3,5-dimethylisoxazol-4-yl)phenol (10g)

To a mixture of **1a** (30 mg, 102 μmol , 1.0 eq) and Et_3SiH (81 μL , 59 mg, 510 μmol , 5.0 eq) was added TFA (0.5 mL). The solution was stirred for 15 min, after which time TLC analysis indicated complete consumption of starting material. The reaction was concentrated *in vacuo* and the residues were dissolved in CH_2Cl_2 (15 mL), washed with a saturated aqueous solution of NaHCO_3 (15 mL), H_2O (15 mL), and brine (15 mL), dried (MgSO_4), filtered, and concentrated *in vacuo*. Purification by silica gel column chromatography (gradient elution, 3 \rightarrow 40% $\text{EtOAc}/40\text{--}60^\circ\text{C}$ petroleum ether) gave **10g** as a pale brown solid (20 mg, 70%); R_f (30% $\text{EtOAc}/\text{petroleum ether}$) 0.24; mp 100–102 $^\circ\text{C}$ (acetone); ν_{max} (thin film)/ cm^{-1} : 3217 (O–H) (br), 3026, 2929, 2852 (C–H) (w), 1632 (m), 1593 (s), 1420 (s), 1325 (s), 1258 (m); $^1\text{H NMR}$ (500 MHz, D_6 -acetone) δ 8.44 (1H, s, OH), 7.35–7.28 (4H, m, C(2'')H, C(6'')H, C(3'')H, C(5'')H), 7.24–7.18 (1H, m, C(4'')H), 6.76–6.73 (1H, m, C(4)H), 6.73–6.71 (1H, m, C(2)H), 6.69–6.66 (1H, m, C(6)H), 3.98 (2H, s, CH_2), 2.38 (3H, s, C(5') CH_3), 2.21 (3H, s, C(3') CH_3); $^{13}\text{C NMR}$ (126 MHz, D_6 -acetone) δ 164.8 (C(5')), 158.0, 157.8 (C(3'), C(1)), 143.7 (C(3)), 141.2 (C(1'')), 131.7 (C(5)), 128.9 (C(2''), C(6'')), 128.4 (C(3''), C(5'')), 126.0 (C(4'')), 120.7 (C(4)), 116.2 (C(4')), 114.9 (C(2)), 113.5 (C(6)), 41.3 (CH_2), 10.7 (C(5') CH_3), 10.0 (C(3') CH_3); HRMS m/z (ES) found $[\text{M} + \text{Na}]^+$ 302.1151; $\text{C}_{18}\text{H}_{17}\text{NNaO}_2$ requires M^+ 302.1151; LRMS m/z (ES $^+$) 280 ($[\text{M} + \text{H}]^+$, 100%), 302 ($[\text{M} + \text{Na}]^+$, 88%); HPLC: RT 12.59 min, purity 97.5% (M1).

4.2.25. [3-(3,5-Dimethylisoxazol-4-yl)-5-hydroxyphenyl](piperidin-1-yl)methanone (11a)

To a solution of **21** (50 mg, 214 μmol , 1.0 eq) in THF was added EDC.HCl (62 mg, 323 μmol , 1.5 eq.) and HOBt hydrate (15 mg, 111 μmol , 0.5 eq). The reaction solution was stirred at rt for 20 min, then piperidine (64 μL , 55 mg, 644 μmol , 3.0 eq). The mixture was then heated at 55 $^\circ\text{C}$ for 3 days, then diluted with EtOAc (5 mL), and washed with H_2O (4 \times 5 mL), and brine (3 \times 5 mL), dried over anhydrous MgSO_4 , filtered, and concentrated *in vacuo*. Purification by silica gel chromatography, eluting with MeOH in CH_2Cl_2 (gradient elution 0 \rightarrow 10%) yielded **11a** (36 mg, 56%) as a colourless solid: R_f (1% AcOH/EtOAc) 0.48; mp 189–191 $^\circ\text{C}$ (MeOH); ν_{max} (thin film)/ cm^{-1} : 3188 (br), 2969 (w), 2925 (w), 2857 (w), 1587 (s), 1432 (s), 1363 (w), 1324 (s), 1303 (med), 1244 (s), 1113 (s), 1071 (w), 1030 (m); $^1\text{H NMR}$ (400 MHz, MeOD) δ 6.82 (1H, dd, $J = 2.1$, 1.5 Hz, C(2)H), 6.79 (1H, dd, $J = 2.1$, 1.5 Hz, C(6)H), 6.77 (1H, dd, $J = 1.5$, 1.5 Hz, C(4)H), 3.77–3.63 (2H, m, CH_2N), 3.50–3.37 (2H, m, CH_2N), 2.42 (3H, s, C(5') CH_3), 2.26 (3H, s, C(3') CH_3), 1.77–1.62 (4H, m, $\text{CH}_2\text{CH}_2\text{N}$ & $\text{CH}_2\text{CH}_2\text{CH}_2\text{N}$), 1.62–1.51 (2H, m, $\text{CH}_2\text{CH}_2\text{N}$); $^{13}\text{C NMR}$ (101 MHz, MeOD) δ 171.7 ($\text{R}_2\text{NCO-Ar}$), 167.2 (C(5')), 159.8 (C(3')), 159.4 (C(1)), 139.3 (C(5)), 133.3 (C(3)), 119.1 (C(4)), 118.3 (C(2)), 117.3 (C(4')), 113.8 (C(6)), 50.0 (CH_2N), 44.3 (CH_2N), 27.6 ($\text{CH}_2\text{CH}_2\text{N}$), 26.7 ($\text{CH}_2\text{CH}_2\text{N}$), 25.4 ($\text{CH}_2\text{CH}_2\text{CH}_2\text{N}$), 11.4 (C(5') CH_3), 10.6 (C(3') CH_3); HRMS m/z (ES $^-$) Found: 299.14015. $\text{C}_{17}\text{H}_{19}\text{N}_2\text{O}_3$ requires M^- 299.1401; LRMS m/z (ES $^+$) 299 ($[\text{M}-\text{H}]^-$, 100%); HPLC: retention time 7.82 min, purity 97.9% (M3).

4.2.26. [3-(3,5-Dimethylisoxazol-4-yl)-5-hydroxyphenyl](morpholin-4-yl)methanone (11b)

To a solution of **21** (50 mg, 214 μmol , 1.0 eq) in THF was added EDC.HCl (62 mg, 323 μmol , 1.5 eq) and HOBt hydrate (15 mg, 111 μmol , 0.5 eq). The reaction was stirred at rt for 20 min, then morpholine (56 μL , 56 mg, 640 μmol , 3.0 eq). The reaction mixture was then heated at 55 $^\circ\text{C}$ for 3 days, then diluted with EtOAc (5 mL), and washed with H_2O (4 \times 5 mL) and brine (3 \times 5 mL), dried over anhydrous MgSO_4 , filtered, and concentrated *in vacuo*. Purification by silica gel chromatography, eluting with MeOH in CH_2Cl_2 (gradient elution 0 \rightarrow 10%) yielded **11b** (34 mg, 52%) as a colourless solid: R_f (10% MeOH/ CH_2Cl_2) 0.28; mp 195–197 $^\circ\text{C}$ (CH_2Cl_2); ν_{max} (thin film)/ cm^{-1} : 3175 (br) 2999 (med), 2937 (w), 2857 (w),

1585 (s), 1473 (m), 1416 (m), 1324 (m), 1253 (m), 1231 (w), 1206 (w), 1116 (w), 1026 (w); $^1\text{H NMR}$ (400 MHz, MeOD) δ 6.85–6.81 (3H, m, C(2)H, C(4)H, C(6)H), 3.84–3.44 (8H, m, 2 \times $\text{OCH}_2\text{CH}_2\text{N}$), 2.40 (3H, s, C(5') CH_3), 2.25 (3H, s, C(3') CH_3); $^{13}\text{C NMR}$ (101 MHz, CDCl_3) δ 171.8 ($\text{R}_2\text{NCO-Ar}$), 167.2 (C(5')), 159.8 (C(3')), 159.4 (C(1)), 138.3 (C(5)), 133.4 (C(3)), 119.3 (C(4)), 118.5 (C(2)), 117.1 (C(4')), 114.1 (C(6)), 67.7 (2 \times $\text{OCH}_2\text{CH}_2\text{N}$), 49.5 ($\text{OCH}_2\text{CH}_2\text{N}$), 43.7 ($\text{OCH}_2\text{CH}_2\text{N}$), 11.4, 10.6; HRMS m/z (ES $^-$) Found: 301.1193. $\text{C}_{16}\text{H}_{17}\text{N}_2\text{O}_4$ requires M^- 301.1194; LRMS m/z (ES $^-$) 301 ($[\text{M}-\text{H}]^-$, 100%). HPLC: RT 6.63 min, purity 97.4% (M3).

4.2.27. Potassium (3,5-dimethylisoxazol-4-yl)trifluoroborate (13)⁵³

Following to the procedure of Lennox et al.,⁵⁴ to a suspension of (3,5-dimethylisoxazol-4-yl)boronic acid (**12**, 2.5 g, 17.74 mmol, 1.0 eq) in CH_3CN (15 mL), was added 7 mL of a 10 M aqueous solution of KF (4.12 g, 70.96 mmol, 4.0 eq). The reaction mixture was stirred at rt until the boronic acid had completely dissolved. A solution of l-(+)-tartaric acid (5.46 g, 36.37 mmol, 2.05 eq) in THF (27 mL) was added dropwise to the reaction mixture over a period of 10 min. A colourless precipitate formed instantly. The suspension was stirred at room temperature for 20 min. After this time the reaction mixture was filtered. The filter cake was rinsed several times with CH_3CN , the combined filtrates were concentrated *in vacuo* to give **13** as a colourless solid (2.62 g, 12.9 mmol, 73%). R_f (petroleum ether: Et_2O 1:1) 0.10; mp > 300 $^\circ\text{C}$ (acetone) [lit. mp > 200 $^\circ\text{C}$]; $^1\text{H NMR}$ (400 MHz, D_6 -DMSO) δ 2.19 (3H, s, C(5') CH_3), 2.04 (3H, s, C(3') CH_3); $^{11}\text{B NMR}$ (160 MHz, D_6 -DMSO) δ 2.33 (q, $J = 49$ Hz); $^{19}\text{F NMR}$ (377 MHz, D_6 -DMSO) δ -134.1 - -134.9 (m); LRMS m/z (ES $^-$) 164 ($[\text{M}-\text{K}]^-$, 82%), 367 ($[\text{2M}-\text{K}]^-$, 100%). Data are in good agreement with literature values.⁵³

4.2.28. 3-Bromo-5-hydroxybenzylalcohol (15)^{20,55}

Following the procedure of Hewings et al.,²⁰ to a solution of 3-bromo-5-hydroxybenzoic acid (5.15 g, 23.7 mmol, 1.0 eq) in anhydrous THF (200 mL) was added a 1 M solution of borane (70.0 mL, 6.02 g, 70.0 mmol, 3.0 eq) in THF dropwise at 0 $^\circ\text{C}$. The reaction solution was warmed to rt and stirred for 44 h, then was cooled to 0 $^\circ\text{C}$. This was followed by slow addition of MeOH (200 mL), then an aqueous 1 M solution of HCl (100 mL), and then the volatile components were removed *in vacuo*. The resulting residue was resuspended in H_2O (150 mL) and extracted with EtOAc (3 \times 150 mL). The combined organic layers were washed with a saturated aqueous solution of NaHCO_3 (450 mL), and brine (450 mL), dried over anhydrous MgSO_4 , filtered, and concentrated *in vacuo* to give **15** (4.65 g, 22.9 mmol, 96%) as an oil that was deemed pure enough for use in the next step: R_f (30% $\text{EtOAc}/\text{petroleum ether}$) 0.22; $^1\text{H NMR}$ (400 MHz, D_6 -DMSO) δ 9.81 (1H, s, C(5)OH), 6.93–6.88 (1H, m, C(2)H), 6.79 (1H, dd, $J = 1.9$, 1.9 Hz, C(4)H), 6.74–6.70 (1H, m, C(6)H), 5.25 (1H, t, $J = 5.7$ Hz, CH_2OH), 4.40 (2H, d, $J = 5.7$ Hz, $\text{CH}_2\text{-OH}$); LRMS m/z (ES $^-$) 201 & 203 ($[\text{M}(^{79}\text{Br})-\text{H}]^-$ & $[\text{M}(^{81}\text{Br})-\text{H}]^-$, 79%), 403 & 405 & 407 ($[\text{M}(^{79}\text{Br})\text{M}(^{79}\text{Br})-\text{H}]^-$ & $[\text{M}(^{79}\text{Br})\text{M}(^{81}\text{Br})-\text{H}]^-$ & $[\text{M}(^{81}\text{Br})\text{M}(^{81}\text{Br})-\text{H}]^-$, 100%). Data are in good agreement with literature values.²⁰

4.2.29. 3-Bromo-5-hydroxybenzaldehyde (16)²¹

To a solution of 3-bromo-5-hydroxybenzylalcohol **15** (1.79 g, 8.77 mmol, 1.0 eq) in CHCl_3 (15 mL) and ethyl acetate (3 mL) was added activated MnO_2 (5.34 g, 61.4 mmol, 7 eq). The reaction mixture was heated under reflux for 3 h after which time the reaction was judged to be complete by TLC analysis. After this time the suspension was cooled to rt and filtered through Celite[®], eluting with CH_2Cl_2 . The volatile components were removed *in vacuo*, and the resulting solid was purified by silica gel chromatography, ethyl acetate: petroleum ether 1:3, to yielded **16** (1.39 g, 78%) as an off-white solid: R_f (30% $\text{EtOAc}/\text{petroleum ether}$) 0.50; mp (from CHCl_3) 137–139 $^\circ\text{C}$ [lit. mp 137–140 $^\circ\text{C}$]; $^1\text{H NMR}$ (400 MHz,

D₆-DMSO) δ 10.45 (1H, s, CHO), 9.86 (1H, s, C(5)OH), 7.52–7.45 (1H, m, C_{Ar}H), 7.30–7.19 (2H, m, 2 \times C_{Ar}H); LRMS m/z (ES⁻) 199 & 201 ([M(⁷⁹Br)–H]⁻ & [M(⁸¹Br)–H]⁻, 31%), 399 & 401 & 403 ([M(⁷⁹Br)M(⁷⁹Br)–H]⁻ & [M(⁷⁹Br)M(⁸¹Br)–H]⁻ & [M(⁸¹Br)M(⁸¹Br)–H]⁻, 100%). Data are in good agreement with literature values.²¹

4.2.30. 3-(3,5-Dimethyl-1,2-oxazol-4-yl)-5-hydroxybenzaldehyde (17)²¹

Na₂CO₃ (1.41 g, 13.3 mmol, 3.0 eq) was ground to fine powder and added together with **16** (0.890 g, 4.43 mmol, 1.0 eq) and **13** (1.36 g, 6.64 mmol, 1.5 eq) into a Schlenk flask. The atmosphere in the Schlenk flask was removed by applying a vacuum and replaced by N₂. This process was repeated three times. Ethanol (4 mL) was added and the mixture was heated to 80 °C for 10–30 min. RuPhos (0.394 g, 0.531 mmol, 0.12 eq) and Pd(OAc)₂ (60 mg, 0.531 mmol, 0.12 eq) were added to a scintillation vial, which was capped with a septum. The atmosphere in the scintillation vial was removed by applying a vacuum and replaced by N₂. This process was repeated three times. Ethanol (2 mL) was added to the scintillation vial and the mixture was stirred until the solution was colored deep red. This solution was transferred from the scintillation vial to Schlenk flask using a syringe. Ethanol (2 mL) was used to transfer the residual catalyst from the scintillation vial to Schlenk flask. The reaction mixture was heated for 1 h at 80 °C. After completion, the reaction mixture was cooled to rt and diluted with ethyl acetate. The volatile components were removed *in vacuo*. The residue was dissolved in ethyl acetate (50 mL). The organic layer was washed with water (3 \times 20 mL). The organic layer was concentrated *in vacuo*. Purification by silica gel chromatography, eluting with EtOAc in petroleum ether (gradient elution 0 \rightarrow 50%) yielded **17** (803 mg, 85%) as a yellow solid. R_f (20% EtOAc/petroleum ether) 0.13; mp (from EtOAc) 184–186 °C [lit. mp 184–187 °C²¹]; ¹H NMR (400 MHz, D₆-acetone) δ 10.02 (1H, s, CHO), 9.11 (1H, br s, C(5)OH), 7.42 (1H, dd, J = 1.4, 1.4 Hz, C(6)H), 7.36 (1H, dd, J = 2.3, 1.4 Hz, C(2)H), 7.15 (1H, dd, J = 2.3, 1.4 Hz, C(4)H), 2.44 (3H, s, C(5')CH₃), 2.26 (3H, s, C(3')CH₃); LRMS m/z (ES⁻) 216 ([M–H]⁻, 100%). Data are in good agreement with literature values.²¹

4.2.31. 3-(3,5-Dimethylisoxazol-4-yl)-5-((triisopropylsilyloxy)benzaldehyde (18)

To a solution of **17** (475 mg, 2.19 mmol, 1.0 eq) and imidazole (420 mg, 6.17 mmol, 2.8 eq) in DMF (2 mL) at 0 °C, was added TIPSCl (500 μ L, 451 mg, 2.34 mmol, 1.1 eq) dropwise. The reaction was allowed to warm to rt, and stirred for 22 h, then was diluted with H₂O (25 mL). The aqueous phase was extracted with EtOAc (3 \times 25 mL) and the combined organic layers were washed with brine (75 mL), dried over anhydrous MgSO₄, filtered, and concentrated *in vacuo*, to yield **18** (683 mg, 84%) as a volatile liquid that was used without purification: R_f (20% EtOAc/ petroleum ether) 0.69; ν_{\max} (thin film)/cm⁻¹: 2946 (s), 2868 (s), 1702 (s), 1590 (s); ¹H NMR (500 MHz, D₆-acetone) δ 10.06 (1H, s, CHO), 7.56–7.54 (1H, m, C(6)H), 7.45–7.42 (1H, m, C(2)H), 7.23–7.20 (1H, m, C(4)H), 2.44 (3H, s, C(5')CH₃), 2.26 (3H, s, C(3')CH₃), 1.42–1.31 (3H, m, 3 \times CH), 1.16 (9H, s, 3 \times CH₃), 1.14 (9H, s, 3 \times CH₃); ¹³C NMR (126 MHz, D₆-acetone) δ 192.6 (CHO), 166.5 (C(5')), 158.8 (C(5)), 157.9(C(3')), 139.7 (C(3)), 134.0 (C(1)), 127.0 (C(2)), 124.6 (C(4)), 119.2 (C(6)), 116.1 (C(4')), 18.2 (3 \times CH), 13.4 (6 \times CH₃), 11.6 (C(5')CH₃), 10.8 (C(5')CH₃); HRMS m/z (ES⁺) Found: 396.1956. C₂₁H₃₁NNaO₃Si⁺ requires [M + Na]⁺, 396.1965; LRMS m/z (ES⁺) 374 ([M + H]⁺, 100%).

4.2.32. Ethyl 3-(3,5-dimethylisoxazol-4-yl)-5-hydroxybenzoate (20)

To a dry 10–20 mL microwave vial were added ethyl 3-bromo-5-hydroxybenzoate (**19**, 500 mg, 2.04 mmol, 1.0 eq), **13** (435 mg, 2.14 mmol, 1.05 eq), Pd(OAc)₂ (5 mg, 20.0 μ mol, 0.01 eq), RuPhos

(29 mg, 61.1 μ mol, 0.03 eq) and anhydrous Na₂CO₃ (649 mg, 6.12 mmol, 3.0 eq). The vial was sealed and purged with nitrogen, before the addition of ethanol (10 mL). The reaction solution was degassed, by bubbling with nitrogen for 40 min, then heated at 90 °C with microwave irradiation for 90 min. The mixture was allowed to cool to rt and filtered through a thin pad of silica gel, eluting with CH₂Cl₂, and the volatile components were removed *in vacuo*. Purification by silica gel chromatography, eluting with Et₂O in petroleum ether (gradient elution 30 \rightarrow 80%) yielded **20** (224 mg, 68%) as a yellow solid: R_f (1% AcOH/EtOAc) 0.53; ν_{\max} (thin film)/cm⁻¹: 3214 (br), 2983 (w), 2935 (w), 1718 (s), 1633 (m), 1421 (m), 1329 (s), 1265 (s), 1235 (s), 1108 (w), 1023 (w); ¹H NMR (400 MHz, MeOD) δ 7.43 (1H, dd, J = 2.4, 1.5 Hz, C(2)H), 7.41 (1H, dd, J = 1.5, 1.5 Hz, C(6)H), 6.97 (1H, dd, J = 2.4, 1.5 Hz, C(4)H), 4.36 (2H, q, J = 7.1 Hz, CH₂CH₃), 2.42 (3H, s, C(5')CH₃), 2.26 (3H, s, C(3')CH₃), 1.39 (3H, t, J = 7.1 Hz, CH₂CH₃); ¹³C NMR (101 MHz, CDCl₃) δ 167.6 (C = O), 167.1 (C(5')), 159.7 (C(5)), 159.3 (C(3')), 133.5 (C(3)), 132.9 (C(1)), 122.0 (C(2)), 121.5 (C(4)), 117.1 (C(6)), 116.2 (C(4')), 62.2 (CH₂CH₃), 14.5 (CH₂CH₃), 11.3 (C(5')CH₃), 10.6 (C(3')CH₃); HRMS m/z (ES⁻) Found: 260.0927. C₁₄H₁₄NO₄ requires M⁻ 260.0928; LRMS m/z (ES⁻) 260 ([M–H]⁻, 100%).

4.2.33. 3-(3,5-Dimethylisoxazol-4-yl)-5-hydroxybenzoic acid (21)

To a solution of **20** (295 mg, 1.13 mmol, 1.0 eq) in THF (5 mL) and H₂O (2.5 mL) was added LiOH (81 mg, 3.38 mmol, 3.0 eq). The reaction mixture was stirred for 25 h, then Et₂O (10 mL) and an aqueous 2 M LiOH solution (10 mL) was added. The phases were separated, and the aqueous phase was washed with Et₂O (2 \times 10 mL), then acidified to pH 3 with an aqueous 1 M HCl solution. The aqueous suspension was then extracted with EtOAc (5 \times 10 mL). The combined organic layers were dried over anhydrous MgSO₄, filtered, and concentrated *in vacuo*, yielding **21** (260 mg, 98%) as a colourless solid: R_f (1% AcOH/EtOAc) 0.53; ν_{\max} (thin film)/cm⁻¹: 3169 (br), 2661 (w), 1695 (s), 1595 (s), 1489 (s), 1325 (s), 1231 (s), 1205 (s), 1078 (w); ¹H NMR (400 MHz, MeOD) δ 7.44 (1H, dd, J = 2.3, 1.5 Hz, C(2)H), 7.43 (1H, dd, J = 1.5, 1.5 Hz, C(6)H), 6.96 (1H, dd, J = 2.3, 1.5 Hz, C(4)H), 2.42 (3H, s, C(5')CH₃), 2.26 (3H, s, C(3')CH₃); ¹³C NMR (101 MHz, CDCl₃) δ 169.3 (C = O), 167.1 (C(5')), 159.8 (C(5)), 159.2 (C(3')), 133.8 (C(3)), 123.8 (C(1)), 122.3 (C(2)), 121.4 (C(4)), 117.2 (C(6)), 116.6 (C(4')), 11.4 (C(5')CH₃), 10.6 (C(3')CH₃); HRMS m/z (ES⁻) Found: 232.0615. C₁₂H₁₂NO₄ requires M⁻ 232.0615; LRMS m/z (ES⁻) 232 ([M–H]⁻, 100%).

4.3. Biological evaluation

4.3.1. Cloning, protein expression and purification

cDNA encoding human BRD4 (NCBI accession numbers NP 055114.1) was obtained from FivePrime and was used as the template to amplify the N-terminal bromodomain region of the protein. Protein expression and purification was carried out as previously described.³⁷ CREBBP was expressed and purified as previously described.²³

4.3.2. Bromodomain AlphaScreen™ assay

Bromodomain AlphaScreen™ assays were carried out as previously described^{20,47} with minor modifications using the following peptide: H4KAc4 peptide (H₂N-YSGRGGK(Ac)GGK(Ac)GLGK(Ac)GGAK(Ac)RHRK(Biotin)-CONH₂). All experiments were carried out in triplicate and OXFBD02 (**1a**) was used as a positive control on every plate. This compound afforded IC₅₀ values in a range from 307 to 358 nM, which is in line with published values [BRD4(1) IC₅₀ = 384 nM²¹]. AlphaScreen™ buffer (25 mM HEPES, 100 mM NaCl, 0.05% w/v CHAPS, 0.1% w/v BSA; pH 7.6) was prepared fresh each day by supplementing HEPES base with BSA, filter sterilisation through a 0.22 μ m filter, and storage at 4 °C, with equilibration to room temperature before use. Biotinylated peptides

employed and final assay concentrations were: his₆BRD4(1) 10 nM, H4[1–20](KAC)₄ 4 nM; donor beads 5 µg/mL; acceptor beads 5 µg/mL; DMSO < 0.5%. Compounds were prepared as 30 mM DMSO stocks. Inhibition was reported as a reduction in signal arising from peptide-bromodomain interaction, with all plates including buffer and DMSO controls. Concentration-response curves against BRD4 were performed in triplicate on a ProxiPlate-384 Plus (Perkin Elmer), which was read using a Perkin Elmer Wallac Multilabel reader 2104. For incubation steps, the plate was sealed, shaken for 10 s at 600 rpm, and incubated at room temperature in the dark for 1 h.

4.3.3. Isothermal titration calorimetry

All calorimetric experiments were performed on a MicroCal PEAQ-ITC Automated (Malvern) and analysed with the MicroCal PEAQ-ITC Analysis software (Malvern 1.1.0.1262) using a single binding site model. The first data point was excluded from the analysis. BRD4(1) was dialysed at 4 °C overnight in a Slide-A-Lyzer[®] MINI Dialysis Device (2000 MWCO; Thermo Scientific Life Technologies) into 50 mM HEPES, 150 mM NaCl containing 0.2% DMSO; pH 7.4. Proteins were centrifuged to remove aggregates (3 min, 3000 rpm, 25 °C). Protein concentrations were determined by measuring the absorbance at 280 nm using a NanoDrop Lite spectrophotometer (Nanodrop[®] Technologies Inc.) by using the predicted protein absorbance (BRD4(1): $\epsilon_{280} = 28420 \text{ M}^{-1} \text{ cm}^{-1}$, CREBBP: $\epsilon_{280} = 26930 \text{ M}^{-1} \text{ cm}^{-1}$). Small molecule ligand were dissolved as 5 to 10 mM DMSO stock solution and diluted to the required concentration using dialysis buffer. The cell was stirred at 750 rpm, reference power set to 5 µcal/s and temperature held at 25 °C. After an initial delay of 60 s, 19 × 2 µL injections (first injection 0.4 µL) were performed with a spacing of 180 s. Heated dilutions were measured under the same conditions and subtracted for analysis. Small molecule solutions in the calorimetric cell (250 µL, (10 to 20 µM)) were titrated with the protein solutions in the syringe (60 µL, 109 to 160 µM).

4.3.4. Crystallisation

Aliquots of the purified proteins were set up for crystallisation using a mosquito[®] crystallisation robot (TTP Labtech, Royston UK). Coarse screens were typically setup onto Greiner 3-well plates using three different drop ratios of precipitant to protein per condition (100 + 50 nL, 75 + 75 nL and 50 + 100 nL). Initial hits were optimised further using Greiner 1-well plates and scaling up the drop sizes in steps. All crystallisations were carried out using the sitting drop vapor diffusion method at 4 °C. BRD4(1) crystals with **9j** (1 mM final concentration) were grown by mixing 200 nL of the protein (7.3 mg/ml) with 100 nL of reservoir solution containing 20% PEG 3350 and 0.1 M citrate pH 5.5. BRD4(1) crystals with **9i** (1 mM final concentration) were grown by mixing 200 nL of the protein (7.3 mg/ml) with an 100 nL of reservoir solution containing 0.1 M K(citrate), 0.1 M cacodylate pH 6.5. BRD4(1) crystals with **10d** (1 mM final concentration) were grown by mixing 200 nL of the protein (6.6 mg/ml) with an 100 nL of reservoir solution containing 24.0% PEG1K and 20.0% glycerol.

4.3.5. Data collection and structure solution

Crystals were cryo-protected using the well solution supplemented with additional ethylene glycol and were flash frozen in liquid nitrogen. Data were collected at Diamond beamline I24 using a Pilatus6M detector at 0.96861 Å. Indexing and integration were carried out using XDS^{56,57} and scaling was performed with SCALA.⁵⁸ Initial phases were calculated by molecular replacement with PHASER⁵⁹ using an ensemble of known bromodomain models (PDB codes 2OSS, 2OUO, 2GRC, 2OO1, 3DAI, 3D7C, 3DWY). Initial models were built by ARP/wARP⁶⁰ and building was completed manually with COOT.⁶¹ Refinement was carried out in REFMAC5.⁶²

Data collection and refinement statistics can be found in [Supplemental Table S6](#). The models and structure factors have been deposited with PDB accession codes: 6FSY (BRD4(1)/ **9j** complex), 6FT3 (BRD4(1)/**9i** complex) and 6FT4 (BRD4(1)/ **10d** complex).

4.3.6. Human microsomal stability assay

These assays were performed by Cyprotex (Nether Alderley, UK) according to standard operating protocols.

4.3.7. Luciferase reporter assay

The NF-κB luciferase reporter plasmid carrying 6 tandem κB-sites, NF-κB-luc, CMV-β-Gal, and pBSSK were generously provided by Dr. Jorge Iñigues-Lluhí (The University of Michigan Pharmacology Department).⁶³ All cells were maintained in 5% CO₂ at 37 °C. HeLa cells were grown in Dulbecco's modified Eagle's medium (DMEM, Invitrogen) supplemented with 10% FBS. For luciferase assays, 4 × 10⁵ cells were seeded in a 6-well dish and allowed to adhere overnight. The media was removed, and cells were transfected in Opti-Mem (Invitrogen) with 400 ng NF-κB-luc, 200 ng CMV-β-Gal, and 1400 ng pBSSK using Lipofectamine 2000 (Life Technologies) according to manufacturer's instructions. After 4.5 h, transfection solution was removed and replaced with DMEM containing 10% FBS. At 24 h after transfection, cells were trypsinized and resuspended in DMEM supplemented with 10% FBS and seeded into a 96-well plate at a density of 8 × 10³ cells per well. After an additional 16 h, media was removed and replaced with Opti-Mem containing vehicle or the indicated compounds delivered in DMSO (1% v/v) at the indicated concentrations. After cells incubated with either vehicle or compound for 1 h, cells were treated with either PBS or IL-1β at a final concentration of 2 ng/mL. After an additional 3 h, media was removed and cells were lysed with 60 µL of passive lysis buffer. Luciferase and β-Galactosidase activities were determined as previously described.⁶⁴ NF-κB luciferase activity and response curve analysis was performed using GraphPad software.

4.3.8. Cell growth assay

Growth inhibition was assessed by sulforhodamine B colorimetric assay as previously described.⁶⁵ Briefly, cells were seeded into 96-well plates at a density appropriate for exponential growth at the start of the assay, and treated with a range of concentrations of OXFBD02 (**1a**) or OXFBD04 (**9j**) for 48 h. Cells were then fixed in 10% (w/v) TCA and stained with sulforhodamine B. The concentrations required to inhibit cell growth by 50% compared to control cells were calculated using GraphPad Prism software (San Diego, CA, USA).

4.3.9. Western blot assay to detect MYC suppression

MCF7 cells were treated with 10 µM of (+)-JQ1, OXFBD04 (**9j**) or OXFBD02 (**1a**) for 10, 24, or 48 h. Cells were lysed in UTB (9 M urea, 75 mM Tris-HCl pH 7.5, 0.15 M β-mercaptoethanol) and briefly sonicated. Protein expression was assessed by immunoblotting with primary antibodies c-myc (Cell Signaling, 5605) and Actin (Santa Cruz, sc-69879), and secondary antibodies IRDye[®] 800CW Donkey anti-Rabbit IgG (H + L) and IRDye[®] 680RD Goat anti-Mouse IgG (H + L) from LI-COR Biosciences. Odyssey IR imaging technology (LI-COR Biosciences) was used for imaging.

4.4. Computational methods

4.4.1. Molecular dynamics

The protein and ligand co-ordinates were taken from the crystal structures of **1a** bound to BRD4(1), where ligand models for **9j** and **9p** were prepared by substituting the atoms of **1a**. The AMBER99SB-IDLN forcefield was used for the protein.⁶⁶ The ligands were protonated at pH 7.4 using the Marvin Suite

16.16.6.0 from ChemAxon (<https://www.chemaxon.com>) and parameterised using the General Amber forcefield (v. 1.8) found in AmberTools16.⁶⁷ All crystallographic water molecules were retained and the TIP3P water model was used.⁶⁸ The system was solvated within a dodecahedral box, with a minimum distance of 1.2 nm between the protein and the edge of the box. Water molecules were substituted with a sodium ion to neutralise the net charge and to maintain an overall salt concentration of 150 mM sodium chloride. The systems were subject to energy minimisation using the steepest decent algorithm, with a maximum force cut off of 100 kJ mol⁻¹ nm⁻¹. The systems then underwent 200 ps equilibration in the isothermal-isobaric ensemble. The temperature was coupled using a Langevin thermostat, with a target temperature of 300 K, and the pressure was coupled using the Berendsen weak coupling algorithm to a target pressure of 1 atm.^{69–71} Simulations were then carried out for 50 ns using GROMACS 2016.4, in triplicate.⁷² Torsions were calculated using the MDAnalysis package for Python and a rolling average calculated over 10 time points.⁷³

Acknowledgments

We thank Dr Angelina Sekirnik and Dr Liam O'Connor for conducting some initial biological experiments in this project. L.E.J. and J.P.B. thank the EPSRC and GlaxoSmithKline for studentship support via the Systems Approaches to Biomedical Sciences Centre for Doctoral Training (EP/G037280/1). M.S. is supported by the Deutsche Forschungsgemeinschaft (SCHI 1408/1-1). D.S.H. thanks Cancer Research UK for a studentship. C.M.C.L. thanks the BBSRC and GlaxoSmithKline for the award of a BBSRC iCASE studentship (BB/M015157/1). A.R.S., J.K.R., and M.M. thank the EPSRC Centre for Doctoral Training in Synthesis for Biology and Medicine (EP/L015838/1) for studentship support, generously supported by AstraZeneca, Diamond Light Source, Defence Science and Technology Laboratory, Evotec, GlaxoSmithKline, Janssen, Novartis, Pfizer, Syngenta, Takeda, UCB, and Vertex. C.N.G.E. thanks Cancer Research UK and the EPSRC for studentship support through the CR-UK and EPSRC Cancer Imaging Centre in Oxford. I.N.M., S.J.C., and E.M.H. thank the MRC (MR/N009460/1) for funding. This project has received funding from the European Union's Horizon 2020 research and innovation programme under grant agreement No 658825. P.F. and S.P. are supported by a Wellcome Trust Career Development Fellowship (095751/Z/11/Z) and the SGC, a registered charity (number 1097737) that receives funds from AbbVie, Bayer Pharma AG, Boehringer Ingelheim, Canada Foundation for Innovation, Eshelman Institute for Innovation, Genome Canada, Innovative Medicines Initiative (EU/EFPIA) [ULTRA-DD grant no. 115766], Janssen, Merck & Co., Novartis Pharma AG, Ontario Ministry of Economic Development and Innovation, Pfizer, São Paulo Research Foundation-FAPESP, Takeda, and the Wellcome Trust (092809/Z/10/Z). The authors would like to thank Diamond Light Source for beamtime (proposal mx15433), and the staff of beamlines I24 for assistance with crystal testing and data collection. We would like to acknowledge the use of the University of Oxford Advanced Research Computing (ARC) facility in carrying out this work: <http://dx.doi.org/10.5281/zenodo.22558>. P.C.B. thanks Lady Margaret Hall, Oxford for research funding. E.M.H. thanks Cancer Research UK (C9720/A18513) for funding. S.J.C. thanks St Hugh's College, Oxford, for research funding.

A. Supplementary data

Supplementary data associated with this article can be found, in the online version, at <https://doi.org/10.1016/j.bmc.2018.05.003>.

References

- Weinert BT, Wagner SA, Horn H, et al. Proteome-wide mapping of the Drosophila acetylome demonstrates a high degree of conservation of lysine acetylation. *Sci Signal*. 2011;4:Ra48.
- Kouzarides T. Acetylation: a regulatory modification to rival phosphorylation? *EMBO J*. 2000;19:1176–1179.
- Strahl BD, Allis CD. The language of covalent histone modifications. *Nature*. 2000;403:41–45.
- Gardner KE, Allis CD, Strahl BD. Operating on chromatin, a colorful language where context matters. *J Mol Biol*. 2011;409:36–46.
- Filippakopoulos P, Knapp S. The bromodomain interaction module. *FEBS Lett*. 2012;586:2692–2704.
- Mujtaba S, Zeng L, Zhou MM. Structure and acetyl-lysine recognition of the bromodomain. *Oncogene*. 2007;26:5521–5527.
- Hewings DS, Rooney TP, Jennings LE, et al. Progress in the development and application of small molecule inhibitors of bromodomain-acetyl-lysine interactions. *J Med Chem*. 2012;55:9393–9413.
- Conway SJ. Bromodomains: are readers right for epigenetic therapy? *ACS Med Chem Lett*. 2012;3:691–694.
- Jennings LE, Measures AR, Wilson BG, Conway SJ. Phenotypic screening and fragment-based approaches to the discovery of small-molecule bromodomain ligands. *Future Med Chem*. 2014;6:179–204.
- Gallenkamp D, Gelato KA, Haendler B, Weinmann H. Bromodomains and their pharmacological inhibitors. *ChemMedChem*. 2014;9:438–464.
- Zhang G, Smith SG, Zhou MM. Discovery of chemical inhibitors of human bromodomains. *Chem Rev*. 2015;115:11625–11668.
- Romero FA, Taylor AM, Crawford TD, Tsui V, Cote A, Magnuson S. Disrupting acetyl-lysine recognition: progress in the development of bromodomain inhibitors. *J Med Chem*. 2016;59:1271–1298.
- Brand M, Measures AM, Wilson BG, et al. Small molecule inhibitors of bromodomain-acetyl-lysine interactions. *ACS Chem Biol*. 2015;10:22–39.
- Theodoulou NH, Tomkinson NC, Prinjha RK, Humphreys PG. Progress in the development of non-BET bromodomain chemical probes. *ChemMedChem*. 2016;11:477–487.
- Palmer WS. Development of small molecule inhibitors of BRPF1 and TRIM24 bromodomains. *Drug Discov Today Technol*. 2016;19:65–71.
- Theodoulou NH, Tomkinson NC, Prinjha RK, Humphreys PG. Clinical progress and pharmacology of small molecule bromodomain inhibitors. *Curr Opin Chem Biol*. 2016;33:58–66.
- Filippakopoulos P, Knapp S. Targeting bromodomains: epigenetic readers of lysine acetylation. *Nat Rev Drug Discov*. 2014;13:337–356.
- Jones PA, Issa JP, Baylin S. Targeting the cancer epigenome for therapy. *Nat Rev Genet*. 2016;17:630–641.
- Fujisawa T, Filippakopoulos P. Functions of bromodomain-containing proteins and their roles in homeostasis and cancer. *Nat Rev Mol Cell Biol*. 2017;18:246–262.
- Hewings DS, Wang M, Philpott M, et al. 3,5-dimethylisoxazoles act as acetyl-lysine-mimetic bromodomain ligands. *J Med Chem*. 2011;54:6761–6770.
- Hewings DS, Fedorov O, Filippakopoulos P, et al. Optimization of 3,5-dimethylisoxazole derivatives as potent bromodomain ligands. *J Med Chem*. 2013;56:3217–3227.
- Hay D, Fedorov O, Filippakopoulos P, et al. The design and synthesis of 5- and 6-isoxazolylbenzimidazoles as selective inhibitors of the BET bromodomains. *MedChemComm*. 2013;4:140–144.
- Rooney TP, Filippakopoulos P, Fedorov O, et al. A series of potent CREBBP bromodomain ligands reveals an induced-fit pocket stabilized by a cation- π interaction. *Angew Chem Int Ed*. 2014;53:6126–6130.
- Hay DA, Fedorov O, Martin S, et al. Discovery and optimization of small-molecule ligands for the CBP/p300 bromodomains. *J Am Chem Soc*. 2014;136:9308–9319.
- Sekirnik Nee Measures AR, Hewings DS, Theodoulou NH, et al. Isoxazole-derived amino acids are bromodomain-binding acetyl-lysine mimics: incorporation into histone H4 peptides and histone H3. *Angew Chem Int Ed Engl*. 2016;55:8353–8357.
- Dawson MA, Prinjha RK, Dittmann A, et al. Inhibition of BET recruitment to chromatin as an effective treatment for MLL-fusion leukaemia. *Nature*. 2011;478:529–533.
- Bamborough P, Diallo H, Goodacre JD, et al. Fragment-based discovery of bromodomain inhibitors part 2: optimization of phenylisoxazole sulfonamides. *J Med Chem*. 2012;55:587–596.
- Seal J, Lamotte Y, Donche F, et al. Identification of a novel series of BET family bromodomain inhibitors: binding mode and profile of I-BET151 (GSK1210151A). *Bioorg Med Chem Lett*. 2012;22:2968–2972.
- Mirguet O, Lamotte Y, Donche F, et al. From ApoA1 upregulation to BET family bromodomain inhibition: discovery of I-BET151. *Bioorg Med Chem Lett*. 2012;22:2963–2967.
- Gehling VS, Hewitt MC, Vaswani RG, et al. Discovery, design, and optimization of isoxazole azepine BET inhibitors. *ACS Med Chem Lett*. 2013;4:835–840.
- Sharp PP, Garnier J-M, Huang DCS, Burns CJ. Evaluation of functional groups as acetyl-lysine mimetics for BET bromodomain inhibition. *MedChemComm*. 2014;5:1834–1842.
- Mirguet O, Lamotte Y, Chung CW, et al. Naphthyridines as novel BET family bromodomain inhibitors. *ChemMedChem*. 2014;9:580–589.

33. McKeown MR, Shaw DL, Fu H, et al. Biased multicomponent reactions to develop novel bromodomain inhibitors. *J Med Chem.* 2014;57:9019–9027.
34. Ran X, Zhao Y, Liu L, et al. Structure-based design of gamma-carboline analogues as potent and specific BET bromodomain inhibitors. *J Med Chem.* 2015;58:4927–4939.
35. Zhao Y, Bai L, Liu L, et al. Structure-based discovery of 4-(6-methoxy-2-methyl-4-(quinolin-4-yl)-9H-pyrimido[4,5-b]indol-7-yl)-3,5-dimethylisoxazole (CD161) as a potent and orally bioavailable BET bromodomain inhibitor. *J Med Chem.* 2017;60:3887–3901.
36. Picaud S, Da Costa D, Thanasopoulou A, et al. PFI-1, a highly selective protein interaction inhibitor, targeting BET bromodomains. *Cancer Res.* 2013;73:3336–3346.
37. Filippakopoulos P, Qi J, Picaud S, et al. Selective inhibition of BET bromodomains. *Nature.* 2010;468:1067–1073.
38. Shoemaker RH. The NCI60 human tumour cell line anticancer drug screen. *Nat Rev Cancer.* 2006;6:813–823.
39. Lucas X, Wohlwend D, Hugle M, et al. 4-Acyl pyrroles: mimicking acetylated lysines in histone code reading. *Angew Chem Int Ed Engl.* 2013;52:14055–14059.
40. Huang B, Yang XD, Zhou MM, Ozato K, Chen LF. Brd4 coactivates transcriptional activation of NF-kappaB via specific binding to acetylated RelA. *Mol Cell Biol.* 2009;29:1375–1387.
41. Zou Z, Huang B, Wu X, et al. Brd4 maintains constitutively active NF-kappaB in cancer cells by binding to acetylated RelA. *Oncogene.* 2014;33:2395–2404.
42. Perkins ND. Post-translational modifications regulating the activity and function of the nuclear factor kappa B pathway. *Oncogene.* 2006;25:6717–6730.
43. Huang B, Yang XD, Lamb A, Chen LF. Posttranslational modifications of NF-kappaB: another layer of regulation for NF-kappaB signaling pathway. *Cell Signal.* 2010;22:1282–1290.
44. Bruno PA, Morriss-Andrews A, Henderson AR, Brooks 3rd CL, Mapp AK. A synthetic loop replacement peptide that blocks canonical NF-kappaB signaling. *Angew Chem Int Ed Engl.* 2016;55:14997–15001.
45. Hill AP, Young RJ. Getting physical in drug discovery: a contemporary perspective on solubility and hydrophobicity. *Drug Discov Today.* 2010;15:648–655.
46. Young RJ, Green DV, Luscombe CN, Hill AP. Getting physical in drug discovery II: the impact of chromatographic hydrophobicity measurements and aromaticity. *Drug Discov Today.* 2011;16:822–830.
47. Philpott M, Yang J, Tumber T, et al. Bromodomain-peptide displacement assays for interactome mapping and inhibitor discovery. *Mol Biosyst.* 2011;7:2899–2908.
48. Jansma A, Zhang Q, Li B, et al. Verification of a designed intramolecular hydrogen bond in a drug scaffold by nuclear magnetic resonance spectroscopy. *J Med Chem.* 2007;50:5875–5877.
49. Houston JB. Utility of in vitro drug metabolism data in predicting in vivo metabolic clearance. *Biochem Pharmacol.* 1994;47:1469–1479.
50. Gottlieb HE, Kotlyar V, Nudelman A. NMR Chemical Shifts of Common Laboratory Solvents as Trace Impurities. *J Org Chem.* 1997;62:7512–7515.
51. Kofron WG, Baclawski LM. Convenient method for estimation of alkyl lithium concentrations. *J Org Chem.* 1976;41:1879–1880.
52. Love BE, Jones EG. The use of salicylaldehyde phenylhydrazone as an indicator for the titration of organometallic reagents. *J Org Chem.* 1999;64:3755–3756.
53. Molander GA, Canturk B. Organotrifluoroborates and monocoordinated palladium complexes as catalysts—a perfect combination for Suzuki-Miyaura coupling. *Angew Chem Int Ed Engl.* 2009;48:9240–9261.
54. Lennox AJ, Lloyd-Jones GC. Preparation of organotrifluoroborate salts: precipitation-driven equilibrium under non-etching conditions. *Angew Chem Int Ed Engl.* 2012;51:9385–9388.
55. Hamann LG, Higuchi RI, Zhi L, et al. Synthesis and biological activity of a novel series of nonsteroidal, peripherally selective androgen receptor antagonists derived from 1,2-dihydropyridono[5,6-g]quinolines. *J Med Chem.* 1998;41:623–639.
56. Kabsch W. Evaluation of single-crystal X-ray-diffraction data from a position-sensitive detector. *J Appl Crystallogr.* 1988;21:916–924.
57. Kabsch W. Automatic-indexing of rotation diffraction patterns. *J Appl Crystallogr.* 1988;21:67–71.
58. Evans P. SCALA – scale together multiple observations of reflections, 3.3.0; MRC Laboratory of Molecular Biology: Cambridge. 2007.
59. McCoy AJ, Grosse-Kunstleve RW, Storoni LC, Read RJ. Likelihood-enhanced fast translation functions. *Acta Crystallogr D.* 2005;61:458–464.
60. Perrakis A, Morris R, Lamzin VS. Automated protein model building combined with iterative structure refinement. *Nat Struct Biol.* 1999;6:458–463.
61. Emsley P, Cowtan K. Coot: model-building tools for molecular graphics. *Acta Crystallogr D.* 2004;60:2126–2132.
62. Murshudov GN, Vagin AA, Dodson EJ. Refinement of macromolecular structures by the maximum-likelihood method. *Acta Crystallogr D.* 1997;53:240–255.
63. Hojfeldt JW, Cruz-Rodriguez O, Imaeda Y, et al. Bifunctional ligands allow deliberate extrinsic reprogramming of the glucocorticoid receptor. *Mol Endocrinol.* 2014;28:249–259.
64. Iniguez-Lluhi JA, Pearce D. A common motif within the negative regulatory regions of multiple factors inhibits their transcriptional synergy. *Mol Cell Biol.* 2000;20:6040–6050.
65. Vichai V, Kirtikara K. Sulforhodamine B colorimetric assay for cytotoxicity screening. *Nat Protoc.* 2006;1:1112–1116.
66. Lindorff-Larsen K, Piana S, Palmo K, et al. Improved side-chain torsion potentials for the Amber ff99SB protein force field. *Proteins Struct Funct Bioinf.* 2010;78:1950–1958.
67. Wang J, Wolf RM, Caldwell JW, Kollman PA, Case DA. Development and testing of a general amber force field. *J Comput Chem.* 2004;25:1157–1174.
68. Jorgensen WL, Chandrasekhar J, Madura JD, Impey RW, Klein ML. Comparison of simple potential functions for simulating liquid water. *J Chem Phys.* 1983;79:926–935.
69. Berendsen HJC, Postma JPM, Vangunsteren WF, Dinola A, Haak JR. Molecular-dynamics with coupling to an external bath. *J Chem Phys.* 1984;81:3684–3690.
70. Goga N, Rzepiela AJ, de Vries AH, Marrink SJ, Berendsen HJC. Efficient algorithms for Langevin and DPD dynamics. *J Chem Theory Comput.* 2012;8:3637–3649.
71. Van Gunsteren WF, Berendsen HJC. A leap-Frog algorithm for stochastic dynamics. *Mol Simulat.* 1988;1:173–185.
72. Abraham MJ, Murtola T, Schulz R, et al. GROMACS: high performance molecular simulations through multi-level parallelism from laptops to supercomputers. *SoftwareX.* 2015;1–2:19–25.
73. Gowers RJ, Linke M, Barnoud J, et al. MDAnalysis: a python package for the rapid analysis of molecular dynamics simulations. Proc 15th Python Sci Conf. 2016; 98–105.